

Minerva Access is the Institutional Repository of The University of Melbourne

Author/s:

Phonsri, W;Macedo, DS;Vignesh, KR;Rajaraman, G;Davies, CG;Jameson, GNL;Moubaraki, B;Ward, JS;Kruger, PE;Chastanet, G;Murray, KS

Title:

Halogen Substitution Effects on N<sub>2</sub>O Schiff Base Ligands in Unprecedented Abrupt Fell Spin Crossover Complexes

Date:

2017-05-23

Citation:

Phonsri, W., Macedo, D. S., Vignesh, K. R., Rajaraman, G., Davies, C. G., Jameson, G. N. L., Moubaraki, B., Ward, J. S., Kruger, P. E., Chastanet, G. & Murray, K. S. (2017). Halogen Substitution Effects on N<sub>2</sub>O Schiff Base Ligands in Unprecedented Abrupt Fell Spin Crossover Complexes. *Chemistry A European Journal*, 23 (29), pp.7052-7065. <https://doi.org/10.1002/chem.201700232>.

Persistent Link:

<https://hdl.handle.net/11343/292871>

## Author Manuscript

**Title:** Halogen substitution effects on N2O Schiff base ligands in unprecedented abrupt Fe(II) spin crossover complexes including one showing symmetry breaking

**Authors:** Keith Murray, PhD; Wasinee Phonsri, PhD; David S Macedo, BSc Hons; Kuduva R Vignesh, PhD; Gopalan Rajaraman, PhD; Casey G Davies, PhD; Guy N L Jameson, PhD; Boujemaa Moubaraki, PhD; Jas Ward, PhD; Paul E Kruger, PhD; Guillaume Chastanet, PhD

This is the author manuscript accepted for publication and has undergone full peer review but has not been through the copyediting, typesetting, pagination and proofreading process, which may lead to differences between this version and the Version of Record.

**To be cited as:** 10.1002/chem.201700232

**Link to VoR:** <https://doi.org/10.1002/chem.201700232>

# Halogen substitution effects on N<sub>2</sub>O Schiff base ligands in unprecedented abrupt Fe(II) spin crossover complexes including one showing symmetry breaking

Wasinee Phonsri,<sup>[a]</sup> David S. Macedo,<sup>[a]</sup> Kuduva R. Vignesh,<sup>[b]</sup> Gopalan Rajaraman,<sup>[c]</sup> Casey G. Davies,<sup>[d]</sup> Guy N. L. Jameson,<sup>[d]</sup> Boujemaa Moubaraki,<sup>[a]</sup> Jas S. Ward,<sup>[e]</sup> Paul E. Kruger,<sup>[e]</sup> Guillaume Chastanet,<sup>[f]</sup> and Keith S. Murray<sup>\*[a]</sup>

**Abstract:** A family of halogen-substituted Schiff base iron(II) complexes, [Fe<sup>II</sup>(qsal-X)<sub>2</sub>], (qsal-X = 5-X-N-(8-quinolyl)salicylaldimines) where X = F (**1**), Cl (**2**), Br (**3**), I (**4**) has been investigated in detail. Compound **1** shows a temperature invariant high spin state while the others all show abrupt spin transitions, at or above room temperature, viz. 295 K (X = I) up to 342 K (X = Br), these being some of the highest  $T_{1/2}$  values obtained, to date, for Fe(II) N/O species. We have recently reported subtle symmetry breaking in [Fe<sup>II</sup>(qsal-Cl)<sub>2</sub>] **2** with two spin transition steps occurring at 308 and 316 K. A photomagnetic study reveals almost fully HS conversion of [Fe<sup>II</sup>(qsal-I)<sub>2</sub>] **4** at low temperature ( $T(\text{LIESST}) = 54$  K). The halogen substitution effects on the magnetic properties, as well as the crystal packing of the [Fe<sup>II</sup>(qsal-X)<sub>2</sub>] compounds and theoretical calculations, are discussed in depth, giving important knowledge for the design of new spin crossover materials. In comparison to the well known iron(III) analogues, [Fe<sup>III</sup>(qsal-X)<sub>2</sub>]<sup>+</sup>, the two extra  $\pi$ - $\pi$  and P4AE interactions found in [Fe<sup>II</sup>(qsal-X)<sub>2</sub>] compounds, are believed to be accountable for the spin transitions occurring at ambient temperatures.

## Introduction

Spin crossover (SCO) materials continue to generate great interest from both fundamental and more applied aspects.<sup>[1]</sup> Fe(II) d<sup>6</sup> and Fe(III) d<sup>5</sup> compounds remain the metal systems of choice. Mixed N/O-donor sets are well known for Fe(III) but are scarce for Fe(II),<sup>[2]</sup> the latter

traditionally involving N-donors within heterocyclic (pyridyl, pyrazolyl, etc.) ligands.<sup>[3]</sup>

For Fe(II) and Fe(III) complexes with the same N<sub>4</sub>O<sub>2</sub> ligand donor sets, the structural and magnetic properties of several complexes have been reported possessing tetradentate ligands with N<sub>2</sub>O<sub>2</sub><sup>2-</sup> coordination.<sup>[4]</sup> However, the octahedral coordination spheres surrounding Fe(II) and Fe(III) were different. A closer comparison has been given for [Fe<sup>II</sup>(pap-NO<sub>2</sub>)<sub>2</sub>](pap-NO<sub>2</sub> = 2-Hydroxy-5-nitrophenyl-(2-pyridyl)-methaneimine) and [Fe<sup>III</sup>(pap)<sub>2</sub>]X (X = ClO<sub>4</sub> and BF<sub>4</sub>) complexes.<sup>[5]</sup> In the present work, we observe the rare occurrence of Fe(II) and Fe(III) bound, separately, to exactly the same N<sub>4</sub>O<sub>2</sub> ligand donor sets within tridentate quinolyl-salicylaldimine (qsal) meridional chelators. This provides a unique opportunity to compare structural, electronic and SCO properties of Fe(II) and Fe(III) complexes having, essentially, the same ligand field.

The qsal ligands have been studied extensively in Fe(III)-SCO<sup>[2f]</sup> systems since [Fe(qsal)<sub>2</sub>]NCS<sub>2</sub> was reported to show one of the widest hysteresis loops for a SCO compound.<sup>[6]</sup> In contrast, there has only been one substituted derivative of Fe(II) reported, [Fe<sup>II</sup>(qsal-NO<sub>2</sub>)<sub>2</sub>](qsal-NO<sub>2</sub> = 5-nitro-N-(8-quinolyl)salicylald-imines), and found to show incomplete SCO.<sup>[5]</sup> Very recently, we have shown that [Fe<sup>II</sup>(qsal-Cl)<sub>2</sub>] **2** exhibits an abrupt two-step SCO above room temperature.<sup>[7]</sup> This indicates that halogen substitution on the qsal ligand has good potential to improve SCO properties within Fe(II)-SCO systems.

In the present work, the halogen substituents in the 5-salicylaldiminate fragment viz qsal-X, where X = F, Cl, Br, I (Figure 1) have been focused upon. In the solid state, the halogen substituents are anticipated to influence the intermolecular interactions between mononuclear metal centres and to therefore effect any cooperative behaviour within the spin transition.<sup>[8]</sup>

Halogen effects on the SCO behaviour have been reported in the Fe(III) compounds, [Fe(qsal-X)<sub>2</sub>]NCS<sub>2</sub>-solvent, and the spin transition temperature,  $T_{1/2}$ , was found to increase on moving from F to Br.<sup>[9]</sup> The effect of the substituents is expected to be more pronounced in Fe(II) than in Fe(III) complexes, as competing effects of anions and solvent molecules are not present in Fe(II) species.

- [a] Dr W. Phonsri, D. S. Macedo, Dr B. Moubaraki, Prof K. S. Murray  
School of Chemistry, Building 23,  
Monash University, Clayton, Victoria, 3800, Australia  
E-mail: keith.murray@monash.edu
- [b] K. R. Vignesh  
IITB-Monash Research Academy, IIT Bombay,  
Mumbai, 400076, India
- [c] Prof G. Rajaraman  
Department of Chemistry, Indian Institute of Technology,  
Mumbai, 400076, India
- [d] C. G. Davies, Dr. G. N. L. Jameson  
Department of Chemistry & MacDiarmid Institute for Advanced  
Materials and Nanotechnology, University of Otago,  
Dunedin, 9054, New Zealand
- [e] Dr J. S. Ward, Prof P. E. Kruger  
Department of Chemistry & MacDiarmid Institute for Advanced  
Materials and Nanotechnology, University of Canterbury,  
Private Bag 4800, Christchurch 8041, New Zealand.
- [f] Dr G. Chastanet  
CNRS, Université de Bordeaux, ICMCB, 87 avenue du Dr. A.  
Schweitzer, Pessac 33608, France

Supporting information for this article is given via a link at the end of the document. **(Please delete this text if not appropriate)**

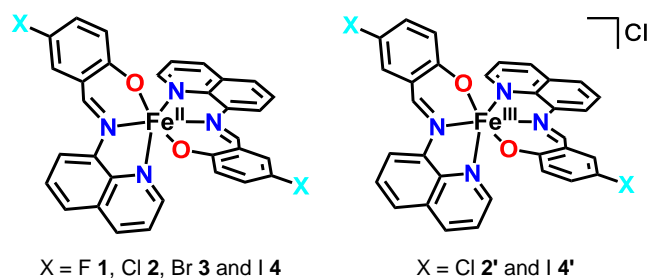


Figure 1 Molecular structures of the qsal-X complexes of iron(II) and iron(III).

With this background in mind, an Fe(II) family of  $[\text{Fe}^{\text{II}}(\text{qsal-X})_2]$  complexes, where  $X = \text{F}$  (**1**),  $\text{Cl}$  (**2**),  $\text{Br}$  (**3**),  $\text{I}$  (**4**) has been synthesized and thoroughly characterized and provides a systematic investigation of these (potentially) SCO materials. Comparisons are made and discussed of the magnetic properties and molecular structures of  $[\text{Fe}^{\text{II}}(\text{qsal-X})_2]$ , with those of the Fe(III) spin crossover analogues,  $[\text{Fe}^{\text{III}}(\text{qsal-I})_2]\text{CF}_3\text{SO}_3$ <sup>[10]</sup> and  $[\text{Fe}^{\text{III}}(\text{qsal-Br})_2]\text{NO}_3 \cdot 2\text{MeOH}$ <sup>[11]</sup> that we have reported previously.

Highlights include the fact that compounds **2-4** all show abrupt SCO transitions at high temperatures that fall between 295 K ( $X = \text{I}$ ) and 342 K ( $X = \text{Br}$ ). These are some of the highest  $T_{1/2}$  values obtained for Fe(II) N/O species. Significantly, we have recently reported<sup>[7]</sup> subtle symmetry breaking and re-entrant<sup>[12]</sup> behaviour in  $[\text{Fe}^{\text{II}}(\text{qsal-Cl})_2]$  **2**, as evidenced by variable temperature crystallographic and magnetic studies. Complex **2** is the first symmetry breaking compound reported in Fe(II)-SCO chemistry possessing an  $\text{N}_2\text{O}$  donor-set.

DFT calculations have also been performed to obtain the spin state energetics and electronic origin of spin crossover behaviour observed in these complexes. Calculations yield very small HS-LS gaps and reproduce the  $T_{1/2}$  values determined by experiment. The  $\pi$ -donor abilities of the halogen substituents at the ligand moiety are found to influence the energies of the  $d_{xz}$  and  $d_{yz}$  orbitals, leading to the difference in the observed SCO characteristics.

## Results and Discussion

### Preparation of $[\text{Fe}(\text{qsal-X})_2]$ and $[\text{Fe}(\text{qsal-X})_2]\text{Cl}$ complexes

A family of Fe(II) complexes,  $[\text{Fe}^{\text{II}}(\text{qsal-X})_2] \cdot n\text{CH}_2\text{Cl}_2$ , where  $n = 0$  and  $X = \text{F}$  **1**,  $\text{Cl}$  **2** and  $\text{Br}$  **3** and where  $n = 1$  and  $X = \text{I}$  **4** has been reproducibly synthesized by layered diffusion of  $\text{CH}_2\text{Cl}_2$  and  $\text{MeOH}$  solutions containing the relevant ligand,  $\text{FeCl}_2$  and  $\text{Et}_3\text{N}$ . After one week, black bar-shaped crystals formed. However, in the case of **2** and **4**, the Fe(III) species  $[\text{Fe}^{\text{III}}(\text{qsal-X})_2]\text{Cl}$  sometimes also co-crystallises from the reaction mixtures on standing for two weeks. Magnetic and PXRD results suggest the presence of both Fe(II)/Fe(III) species in these instances.  $[\text{Fe}(\text{qsal-I})_2]\text{Cl}$  **4'** appears in the same reaction mixture that yields **4** after the latter crystals had been left to sit in the mother

liquor for 2 weeks. However, this was difficult to reproduce. We also believe that the concomitant formation of an Fe(III) compound occurred during the synthesis of **2**, as indicated by the magnetic and PXRD studies. Unfortunately, after many attempts, single crystals of the Fe(III) complex, **2'**, could not be obtained from the synthesis of **2**. Therefore, the direct synthesis of  $[\text{Fe}(\text{qsal-Cl})_2]\text{Cl} \cdot 1.5\text{MeOH} \cdot 1.5\text{H}_2\text{O}$  **2'** was conducted independently. The degree of solvation might differ from the Fe(III) complex formed during the synthesis of **2**, but the Fe(III) moieties are believed to be the same (see PXRD study).

### Structural analysis for $[\text{Fe}(\text{qsal-X})_2]$ and $[\text{Fe}(\text{qsal-X})_2]\text{Cl}$ complexes

Single crystal structures for many of the compounds were obtained at multiple temperatures and yielded information about both the LS and HS phases. The crystallographic data are gathered together in **Fehler! Verweisquelle konnte nicht gefunden werden.** Compound  $[\text{Fe}^{\text{II}}(\text{qsal-F})_2]$  **1**, crystallizes in the trigonal space group  $P3_22_1$  at 123 K.  $[\text{Fe}^{\text{II}}(\text{qsal-Cl})_2]$  **2** was examined at six temperatures, viz. 100, 298, 308, 312, 318 and 330 K and, interestingly, it shows symmetry breaking. Details of the crystallography, symmetry breaking and re-entrant behaviour for **2** have been reported.<sup>[7]</sup> The structure of  $[\text{Fe}^{\text{II}}(\text{qsal-Br})_2]$  **3** was measured at 100 and 380 K with the crystal remaining in the same monoclinic  $P2_1/n$  space group. Complex **4** crystallized in the triclinic space group,  $P\bar{1}$ . At 100 K, **4** exists as  $[\text{Fe}^{\text{II}}(\text{qsal-I})_2] \cdot \text{CH}_2\text{Cl}_2$  while, at room temperature, the crystal data shows that the partial loss of  $\text{CH}_2\text{Cl}_2$  had occurred giving rise to  $[\text{Fe}^{\text{II}}(\text{qsal-I})_2] \cdot 0.3\text{CH}_2\text{Cl}_2$ . Unfortunately, the single crystal data of **4** could not be obtained at 330 K since the crystals lost crystallinity, presumably due to further de-solvation. Slow temperature ramp rates were therefore attempted ( $1 \text{ K min}^{-1}$ ), however, degradation of the crystal was consistently observed. For the Fe(III) complexes,  $[\text{Fe}^{\text{III}}(\text{qsal-Cl})_2]\text{Cl} \cdot 1.5\text{MeOH} \cdot 1.5\text{H}_2\text{O}$  **2'** and  $[\text{Fe}^{\text{III}}(\text{qsal-I})_2]\text{Cl}$  **4'**, the crystals are all in the triclinic,  $P\bar{1}$  system at low temperatures.

The asymmetric units of **3** and **4** contain a neutral molecule of  $[\text{Fe}^{\text{II}}(\text{qsal-X})_2]$ . In the case of **4**, a disordered dichloromethane solvent molecule also appears in the lattice. A molecule of  $[\text{Fe}^{\text{II}}(\text{qsal-Cl})_2]$  is observed in the asymmetric unit of **2** in the monoclinic system at 100, 298, 318 and 330 K. Unexpectedly, when the space group changed to triclinic, at 308 and 312 K, there are two molecules with different spin states (*vide infra*) in the asymmetric unit (Figure 2). In contrast, in compound **1**, only half a molecule is present with only half occupancy of Fe(II). For compounds **2'** and **4'**, a cationic molecule of  $[\text{Fe}^{\text{III}}(\text{qsal-X})_2]^+$  exists together with a counter anion,  $\text{Cl}^-$ . In the case of **4'**, there are two chloride anions each of a half occupancy (Figure S1), whilst only one  $\text{Cl}^-$  site with full occupancy is present in **2'** together with some disordered methanol and water solvate molecules.

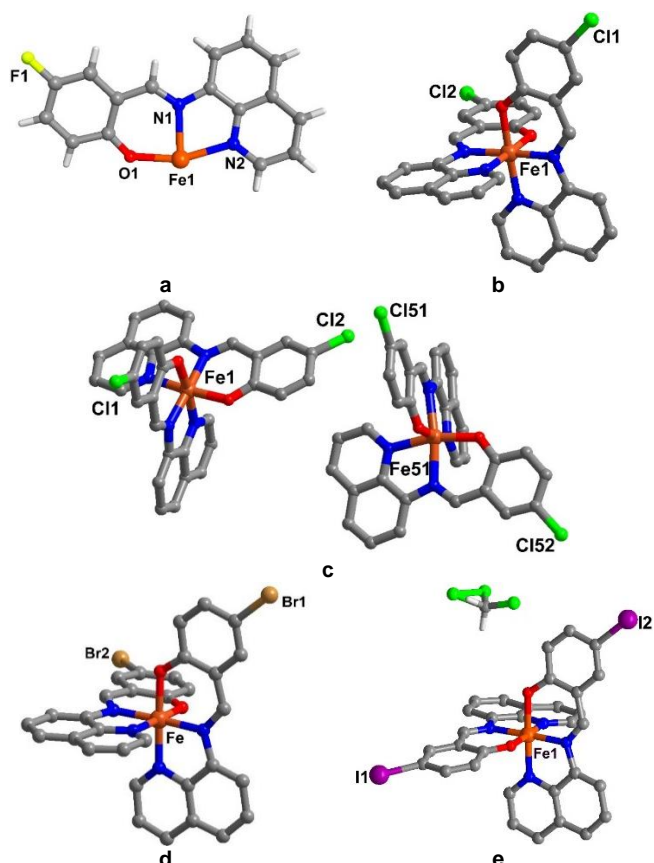


**Figure 2** The asymmetric unit components for a) **1** at 123 K, b) **2** at 100 K, c) **2** at 308 K, d) **3** at 100 K and e) **4** at 100 K. Full atom labelling is shown in the ESI Figure S1. Color code : orange, iron; red , oxygen; dark blue, nitrogen; grey, carbon; yellow in a) fluorine; green in b) and c) chlorine; brown in d) bromine and purple in e) iodine

In all complexes, the Fe centres coordinate to  $N_4O_2$  donors from two tridentate  $qsal-X^-$  ligands chelating in a meridional fashion. Fe-L bond lengths for the compounds are presented in

Table 2. At 100 K, Fe-O and Fe-N distances for **2**,<sup>[7]</sup>**3** and **4** fall between 1.944-1.964 Å and 1.938-1.989 Å, respectively. The same Fe-L regions are also observed in compound **2** collected at 298 K. The octahedral distortion parameters<sup>[13]</sup>  $\Sigma$  (32-41°) and  $\Theta$  (62-74°) of the compounds are small in magnitude. These data indicate that the Fe(II) centres are in LS states.<sup>[14]</sup> The structure of compound **1** at 123 K, with Fe-L bond lengths (Fe-O<sub>av</sub> = 2.016 and Fe-N<sub>av</sub> = 2.178 Å) and octahedral distortion parameters ( $\Sigma$  = 87° and  $\Theta$  = 256°) are typical for Fe(II) in a HS state.<sup>[5, 15]</sup> At higher temperature, 330, 380 and 298 K for compound **2**, **3** and **4**, respectively, the Fe-L bond lengths are in the same range as those noted for **1**. These Fe-L bond lengths increase by about 0.05 and 0.2 Å for Fe-O and Fe-N bonds, respectively. They correspond to octahedral distortion parameter differences, especially  $\Delta\Theta_{HS-LS}$ , of about 130. These data strongly suggest the Fe(II) centres are in the HS state at high temperature and, thus, spin crossover occurs in compounds **2**, **3** and **4**. For the Fe(III) complexes, **2'** and **4'**, the Fe-L bond lengths at 123 and 100 K, respectively, are shown in Table S2 and are typical for HS Fe(III).<sup>[2f, 16]</sup>

### Crystal packing and intermolecular interactions

As mentioned above, for compound **1**, the crystal belongs to the trigonal space group  $P3_22_1$  and the asymmetric unit contains only half of the  $[Fe(qsal-F)_2]$  molecule. This is different from what has been reported previously for  $[Fe^{III}(qsal-F)_2]Y$  complexes ( $Y = \text{anions}$ )<sup>[9, 17]</sup> that usually crystallize in the triclinic  $P\bar{1}$  space group and contain two molecules of Fe(III) compounds in the asymmetric unit. The  $[Fe(qsal-F)_2]$  molecules in **1** form a *pseudo* 3D packing arrangement involving only a few interactions *i.e.*  $\pi$ - $\pi$  and C-H $\cdots$ O/F interactions (Table S3 and Figure S2). It is interesting to note that the packing of Fe complexes with  $qsal-F^-$  ligands strongly depend on the oxidation state of the metal centres and thus the presence of anions. When anions are present, in Fe(III) derivatives, the Fe(III) moieties stack in a zigzag planar fashion with the anions disposed in between the layers<sup>[9]</sup> and they usually exhibit incomplete spin crossover behaviour.<sup>[9, 17]</sup> In contrast, in compound **1** that doesn't possess an anion, the close packing involves only a few interactions possibly leading to HS behaviour only up to 360 K. However, it is noted that HS ground states are generally preferred in Fe(II) compound with an  $N_4O_2$  environment. Therefore, the HS state in **1** can be due to either the electronic structure or to the crystal packing.

Extended structures of the monoclinic compounds **2** and **3** are identical and are therefore discussed together. It is not surprising that the unit cell volume of **3** is larger than that of **2**, by about 91 Å<sup>3</sup> at 100 K. The unit cell parameters for **2** and **3** are comparable, particularly the *a* and *b* parameters. The *c* parameters are significantly larger by about 0.56 Å (19.940 and 19.378 Å for X = Br and Cl, respectively). This is because the orientation of the  $Hqsal$  ligands that have Cl and Br substituents are arranged along the *c* axis. Consequently the size of the halogen substituent influences the larger cell in **3** especially along the *c* axis (Figure S3).

Unlike **1**, the packing in **2** and **3** is typical of Fe- $qsal$  systems that are generally found in Fe(III) complexes.<sup>[2f, 10-11, 18]</sup> Thus, a chain of Fe(II) moieties interact through two sets of  $\pi$ - $\pi$  interactions *via*  $sal\cdots$ quin rings of the  $qsal-X$  ligands and C-H $\cdots$ O interactions along the *b* axis. Moreover, along the *a* axis, C-H $\cdots$ X interactions and two sets of parallel fourfold aryl embraces (P4AE) interactions<sup>[19]</sup> are observed to link the Fe moieties into higher dimensions. P4AE is believed to be the reason for the observation of complete abrupt spin crossover in **2** and **3**.<sup>[2f, 20]</sup> (see magnetic section). Furthermore, in the *ac* plane, there are C-H $\cdots$ Br and an extra two sets of  $\pi$ - $\pi$  interactions holding the Fe molecules in a plane (Figure 3Fehler! Verweisquelle konnte nicht gefunden werden.). Notably, the C2-H2 $\cdots$ Cl1 interaction is absent in compound **2**. These observations agree with the trend observed by both experimental and theoretical studies that van der Waals overlap between phenyl rings is more pronounced for Br than Cl substituents.<sup>[21]</sup> As a short intermolecular contact is known to correlate with the cooperative nature of spin crossover,<sup>[2g, 22]</sup> the lack of C2-H2 $\cdots$ Cl1 interaction possibly results in the lower spin transition temperature in **2** compared to **3** (see magnetism

**Table 1** Crystallographic data and structure refinement for **1 - 4** at various temperatures

	<b>1</b>		<b>2</b>						<b>3</b>		<b>4</b>	
	<b>123 K</b>	<b>100 K</b>	<b>298 K</b>	<b>308 K</b>	<b>312 K</b>	<b>318 K</b>	<b>330 K</b>	<b>100 K</b>	<b>380 K</b>	<b>100 K</b>	<b>298 K</b>	
Formula	C <sub>32</sub> H <sub>20</sub> F <sub>2</sub> FeN <sub>4</sub> O <sub>2</sub>	C <sub>32</sub> H <sub>20</sub> Cl <sub>2</sub> FeN <sub>4</sub> O <sub>2</sub>	C <sub>32</sub> H <sub>20</sub> Cl <sub>2</sub> FeN <sub>4</sub> O <sub>2</sub>	C <sub>32</sub> H <sub>20</sub> Cl <sub>2</sub> FeN <sub>4</sub> O <sub>2</sub>	C <sub>32</sub> H <sub>20</sub> Cl <sub>2</sub> FeN <sub>4</sub> O <sub>2</sub>	C <sub>32</sub> H <sub>20</sub> Cl <sub>2</sub> FeN <sub>4</sub> O <sub>2</sub>	C <sub>32</sub> H <sub>20</sub> Cl <sub>2</sub> FeN <sub>4</sub> O <sub>2</sub>	C <sub>32</sub> H <sub>20</sub> Br <sub>2</sub> FeN <sub>4</sub> O <sub>2</sub>	C <sub>32</sub> H <sub>20</sub> Br <sub>2</sub> FeN <sub>4</sub> O <sub>2</sub>	C <sub>33</sub> H <sub>22</sub> Cl <sub>2</sub> FeI <sub>2</sub> N <sub>4</sub> O <sub>2</sub>	C <sub>32.30</sub> H <sub>20.60</sub> Cl <sub>0.60</sub> FeI <sub>2</sub> N <sub>4</sub> O <sub>2</sub>	
Molecular weight / gmol <sup>-1</sup>	586.37	619.27	619.27	619.27	619.27	619.27	619.27	708.19	708.19	887.10	827.65	
Crystal system	Trigonal	Monoclinic	Monoclinic	Triclinic	Triclinic	Monoclinic	Monoclinic	Monoclinic	Monoclinic	Triclinic	Triclinic	
Space group	P3 <sub>2</sub> 1	P2 <sub>1</sub> /n	P2 <sub>1</sub> /n	P1	P1	P2 <sub>1</sub> /n	P2 <sub>1</sub> /n	P2 <sub>1</sub> /n	P2 <sub>1</sub> /n	P1	P1	
a / Å	11.9101 (3)	10.2044 (2)	10.2113 (2)	10.2926 (5)	10.3266 (6)	10.3632 (3)	10.3970 (4)	10.238 (2)	10.5291 (4)	11.990 (2)	11.941 (2)	
b / Å	11.9101 (3)	12.8835 (2)	12.9889 (2)	13.0726 (5)	13.1023 (6)	13.1281 (3)	13.1513 (4)	12.922 (3)	13.2185 (6)	12.580 (3)	12.649 (3)	
c / Å	15.2216 (3)	19.3776 (4)	19.6876 (4)	19.6371 (8)	19.6014 (9)	19.5466 (5)	19.5205 (6)	19.940 (4)	19.9114 (11)	12.770 (3)	12.889 (3)	
α / °	90	90	90	90.988 (3)	90.696 (4)	90	90	90	90	119.07 (3)	118.14 (3)	
β / °	90	93.6752 (18)	93.2672 (18)	93.801 (3)	93.869 (4)	94.034 (3)	94.140 (3)	93.40 (3)	94.244 (4)	98.29 (3)	97.96 (3)	
γ / °	120	90	90	90.596 (3)	90.429 (4)	90	90	90	90	107.07 (3)	105.44 (3)	
Cell volume / Å <sup>3</sup>	1869.91 (8)	2542.30 (9)	2606.99 (9)	2635.81 (19)	2645.8 (2)	2652.71 (12)	2662.15 (15)	2633.3 (9)	2763.6 (2)	1511.6 (5)	1572.8 (5)	
Z	3	4	4	4	4	4	4	4	4	2	2	
Reflections collected	30055	17188	18456	19835	20178	19430	19362	31602	23162	26864	23665	
Independent reflections, R <sub>int</sub>	3783, 0.0857	5085, 0.0477	5228, 0.0436	10745, 0.0424	10788, 0.0518	5512, 0.0458	5544, 0.0501	7638, 0.1095	5476, 0.0620	7114, 0.0326	6237, 0.0798	
Restraints/parameters	0/186	0/370	0/370	0/739	0/739	0/370	0/370	0/370	0/370	9/407	9/406	
Goodness-of-fit	0.823	1.020	1.043	1.019	0.998	1.036	1.040	1.040	1.050	1.062	1.064	
Final R indices [I > 2σ(I)]: R <sub>1</sub> , wR <sub>2</sub>	0.0390, 0.0880	0.0437, 0.1186	0.0436, 0.1215	0.0655, 0.2002	0.0673, 0.2083	0.0452, 0.1314	0.0483, 0.1431	0.0636, 0.1918	0.0890, 0.2779	0.0437, 0.1059	0.0865, 0.2621	
CCDC No.	1495815	1495808	1495809	1495810	1495811	1495812	1495813	1495806	1495807	1495816	1495817	

**Table 2** Selected bond lengths and octahedral distortion parameters

	<b>1</b>		<b>2</b>						<b>3</b>		<b>4</b>	
	<b>123 K</b>		<b>100 K</b>	<b>298 K</b>	<b>308 K</b>	<b>312 K</b>	<b>318 K</b>	<b>330 K</b>	<b>100 K</b>	<b>380 K</b>	<b>100 K</b>	<b>298 K</b>
Fe1-O1/Å	2.016 (2)	Fe1-O1/Å	1.955 (2)	1.963 (2)	1.968 (3)	1.979 (3)	1.996 (2)	2.005 (2)	1.944 (3)	2.007 (6)	1.953 (3)	1.997 (5)
Fe1-O1'/Å	2.016 (2)	Fe1-O2/Å	1.959 (2)	1.961 (2)	1.954 (4)	1.969 (4)	2.004 (3)	2.013 (3)	1.946 (3)	2.000 (7)	1.957 (3)	2.017 (6)
Fe1-N1/Å	2.170(2)	Fe1-N1/Å	1.940 (2)	1.961 (2)	2.001 (3)	2.029 (3)	2.096 (2)	2.113 (2)	1.942 (3)	2.137 (7)	1.938 (3)	2.108 (5)
Fe1-N1'/Å	2.170 (2)	Fe1-N2/Å	1.949 (2)	1.983 (2)	2.028 (3)	2.066 (4)	2.128 (2)	2.158 (2)	1.952 (3)	2.157 (8)	1.949 (3)	2.126 (6)
Fe1-N2/Å	2.187 (2)	Fe1-N3/Å	1.956 (2)	1.962 (2)	1.995 (3)	2.028 (4)	2.089 (2)	2.112 (2)	1.946 (3)	2.133 (6)	1.938 (3)	2.096 (5)
Fe1-N2'/Å	2.187 (2)	Fe1-N4/Å	1.937 (2)	1.989 (2)	2.030 (3)	2.066 (4)	2.131 (2)	2.158 (3)	1.961 (3)	2.164 (7)	1.948 (3)	2.132 (6)
		Fe51-O51/Å			1.993 (3)	2.006 (3)						
		Fe51-O52/Å			2.005 (4)	2.007 (4)						
		Fe51-N51/Å			2.085 (3)	2.090 (4)						
		Fe51-N52/Å			2.133 (3)	2.139 (3)						
		Fe51-N53/Å			2.089 (3)	2.096 (4)						
		Fe51-N54/Å			2.131 (4)	2.138 (4)						
Σ/°	87	Σ/° (Fe1, Fe51)	34	32	38, 61	45, 63	62	69	34	74	41	65
Θ/°	256	Θ/° (Fe1, Fe51)	65	74	94, 176	119, 184	178	199	65	209	62	186

section). Further details of the intermolecular interactions present in **2** and **3** are shown in Table S4. As mentioned in the previous work, these two types of P4AE interactions and the extra two sets of  $\pi$ - $\pi$  interactions described here are possibly responsible for the exceptional high spin transition temperatures observed in the complexes (*vide infra*)<sup>[7]</sup>, but

further examples are required to see if these correlations are specific to the X-qsal systems or more broadly applicable.

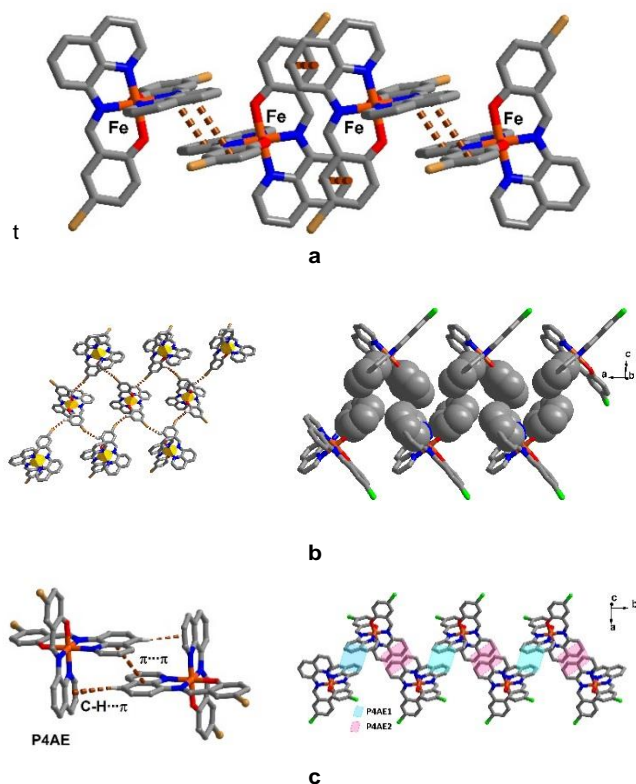


**Figure 3** Representations of a)  $\pi$ - $\pi$  interactions (dotted lines) connecting Fe complex molecules into a chain. b) C-H...Br and  $\pi$ - $\pi$  interactions connecting in a plane along the c axis. c) two sets of P4AE interactions present in **2** and **3**. The colour coding is as shown in Fig. 2.

In regard to the monoclinic structures at various temperatures, it is well known that the unit cell is larger when the spin state of Fe(II) centres changes from LS towards HS with about a 3-4 % increase in cell volume from the primary cell at LS.<sup>[2b]</sup> The unit cell volumes of **2** and **3** at high temperature, for HS states, increase by about 120 Å<sup>3</sup> (ca. 4.7%) and 130 Å<sup>3</sup> (ca. 4.9%), respectively. These % changes in unit cell volume are more than those reported in any Fe(III)-qsal compound<sup>[10-11, 18a]</sup> and in Fe(II) complexes with N<sub>2</sub>O tridentate ligand<sup>[14b, 23]</sup> which undergo complete SCO.

In the case of **4**, the crystal structures were obtained at 100 and 298 K. The overall packing for the LS and HS forms are identical. The Fe(II) moieties interact through P4AE and two sets of  $\pi$ - $\pi$  interactions in a similar way to those observed in **2** and **3**. Details of intermolecular interactions in **4** are summarized in Table S6. While it might have been expected to see differences at 100 K and 298 K, the latter with significantly less solvent molecules present, the packing is the same. Interestingly, instead of the C-

X...H interactions found in **2** and **3**, there are C-I... $\pi$  interactions present that hold two  $\pi$ - $\pi$  chains together in a sheet motif. This, again, agrees with the trend reported by Mooibroek and Gamez.<sup>[21]</sup> They found that the iodine atom shows greater proficiency for halogen bonding to the  $\pi$ -system than other halogens.<sup>[21]</sup> C-I... $\pi$  interactions result in a different type of packing of the layer *i.e.* ABAB for **2**, **3** and AAAA for **4**, respectively (Figure S5). However, this unique packing in a sheet of **4** is a minor difference since the overall packing, in another view, is still similar to that in compounds **2** and **3** (Figure S5). It is worth mentioning, again, that either C-H...X or C-I... $\pi$  interactions are found in compound **1-4**. However, with an absence of P4AE and two sets of  $\pi$ - $\pi$  interactions, **1** exhibits a temperature invariant HS state while **2**, **3** and **4** show abrupt SCO (details given in magnetism section). These results suggest that  $\pi$ - $\pi$  and P4AE interactions significantly impact the presence of abrupt SCO transitions in this family.<sup>[2f, 6, 24]</sup>

Apart from the disorder over the solvents and anions, the packing in the Fe(III) crystals of **2'** and **4'** are identical and distinct from those in the related Fe(II) complexes. There are two sets of  $\pi$ - $\pi$  interactions in a chain motif. In addition to two set of sal-quin  $\pi$ - $\pi$  interactions, as found in **2**, **3** and **4**,  $\pi$ - $\pi$  interactions in **2'** and **4'** are the related sal-quin and quin-quin (Figure 4). This results in an unsymmetrical  $\pi$ - $\pi$  chain in the structures. These chains further link *via* C-X...O and  $\pi$ - $\pi$  interactions (sal-sal rings) and create the channel for chloride anions and solvents in the case of **2'** (Figure S6). Although P4AE interactions are observed to connect Fe(III) moieties along the c axis, the magnetic study shows temperature invariant HS Fe(III) behaviour. This suggests that not only P4AE interactions but also symmetrical  $\pi$ - $\pi$  chains are required in the structures to lead to abrupt SCO transitions. It is noted that electrostatic interaction between [Fe(qsal-X)<sub>2</sub>]<sup>+</sup> cationic and chloride anionic species through C-H...Cl<sup>-</sup> interactions (Table S7) appear to have insignificant impact as they do not improve the magnetic properties of Fe(III) over Fe(II) compounds.

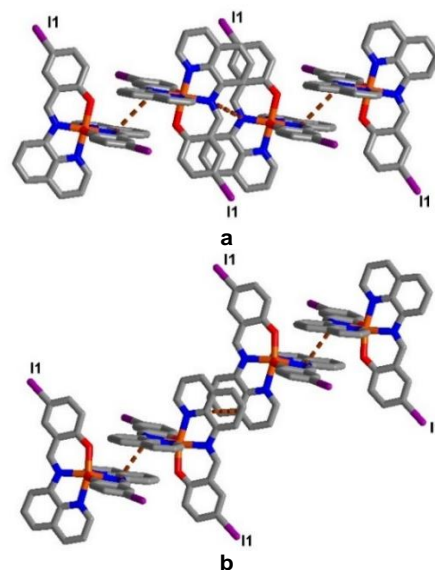


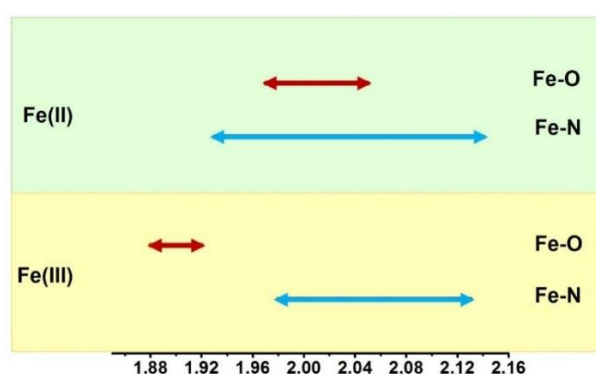
**Figure 4** Two set of  $\pi$ - $\pi$  interactions in a) **4** (symmetrical, two sets from sal-quin) and b) **4'** (un-symmetrical, one set from sal-quin and one set from quin-quin). The colour coding is as shown in Fig. 2.

## Fe-L bond length study in Fe(II) and Fe(III) complexes

Fe-L distances are valuable data for predicting the spin state of the metal centres as well as the occurrence of spin crossover. Thus, the Fe-L bond lengths for LS and HS of Fe(II) and Fe(III) complexes with N<sub>2</sub>O tridentate ligand system are now analyzed. The average bond distances (Fe-L<sub>ave</sub>) of Fe(II) species have been reviewed in Table S8. For Fe(III) complexes, the data were obtained from a recent review by Harding.<sup>[21]</sup> The Fe-L<sub>ave</sub> values were calculated from all available crystal structures while the  $\Delta$ Fe-L<sub>ave</sub> values are calculated from structures reported for both LS and HS solely.

According to the data in

Scheme 1, the  $\Delta$ Fe-N and Fe-N ranges are similar for Fe(II) and Fe(III), however, the Fe(II)-N bonds are slightly shorter in the LS state. On the other hand, Fe-O bonds are significantly weaker in Fe(II) complexes. The Fe(II)-O bond lengths in LS states are longer than Fe(III)-O in HS states by about 0.06 Å. Moreover, there is a greater change observed in  $\Delta$ Fe-O distances for Fe(II) spin crossover complexes than those of Fe(III). Interestingly for the LS state, Fe-O<sub>ave</sub> bonds are weaker than Fe-N<sub>ave</sub> in Fe(II) but stronger for Fe(III) complexes.



Complexes	Fe-O <sub>ave</sub> LS	Fe-O <sub>ave</sub> HS	Fe-N <sub>ave</sub> LS	Fe-N <sub>ave</sub> HS	$\Delta$ Fe-O	$\Delta$ Fe-N
Fe(II)	1.974	2.047	1.927	2.143	0.067	0.141
Fe(III)	1.883	1.916	1.977	2.126	0.038	0.152

**Scheme 1** The average Fe-L and  $\Delta$ Fe-L distances for Fe(II) and Fe(III) complexes with N<sub>2</sub>O tridentate ligands in Å

## Magnetic susceptibility results

The variable-temperature magnetic susceptibility data for the complexes were obtained between 100–400 K using various temperature scan rates *i.e.* 2, 5 and 10 K/min. The magnetic results for the compounds are independent of the scan rate and are illustrated in Figure 5. For **1**, the steady  $\chi_M T$  value of about 3.3 cm<sup>3</sup> K mol<sup>-1</sup> agrees with the single crystal structure and indicates that the HS Fe(II) state exists at all temperatures (Figure S7). At first glance (Figure 5a), **2**, **3** and **4** all show abrupt spin crossover at or above room temperature. However, upon closer inspection, together with DSC results, two steps have been detected in **2** with a *pseudo*-plateau that has a width of about 8 K. Upon heating from 100 K up to 250 K, the  $\chi_M T$  values of **2**, **3** and **4** are invariant to temperature with  $\chi_M T$  values of about 0.3 cm<sup>3</sup> K

mol<sup>-1</sup> indicative of the LS Fe(II) forms. Upon further warming, the spin transition takes place at  $T_{1/2} = 295$  and 342 K for X = I **4** and Br **3**, respectively, while **2** shows a two-step transition at  $T_{1/2} = 308$  and 316 K for the 1<sup>st</sup> and 2<sup>nd</sup> steps, respectively, before reaching the fully HS form at high temperatures. There is a small thermal hysteresis of about 1-2 K width present in these compounds. The magnetic profiles are reproducible in subsequent cycles. The difference in degree of CH<sub>2</sub>Cl<sub>2</sub> solvation noted in the crystal structures at 100 K and 298 K (*vide infra*) does not appear to influence the  $\chi_M T$  plot (Figure 5a), unless the plot is due to the partially desolvated phase.

According to the reviewed data in Table 3, there is only a small number of examples of Fe(II) with N<sub>2</sub>O tridentate ligands that has been characterized. This is perhaps not surprising as the N<sub>4</sub>O<sub>2</sub> environment is generally suitable for Fe(III) SCO and not Fe(II).<sup>[3c, 16, 25]</sup> It is, therefore, rather unexpected for [Fe(qsal-X)<sub>2</sub>] compounds to be able to exhibit complete-abrupt SCO in both Fe(III)<sup>[10-11]</sup> and, especially, Fe(II) oxidation states, with such high  $T_{1/2}$  values. To the best of our knowledge, [Fe(qsal-Br)<sub>2</sub>] shows thermal SCO at the highest spin transition temperature not only in the qsal<sup>-</sup> ligand family<sup>[21]</sup> but also in any Fe(II)-N<sub>2</sub>O tridentate ligand system. Furthermore, [Fe(qsal-Cl)<sub>2</sub>] is the first Fe(II) complex with an N<sub>2</sub>O ligand that exhibits symmetry breaking involving a two-step SCO, above RT.<sup>[7, 11-12, 26]</sup>

Regarding the summary in Table 4, significant supramolecular contacts *i.e.* two sets of symmetrical  $\pi$ - $\pi$  (the same types of originated aromatic rings) and P4AE interactions are believed to be responsible for the abrupt SCO in **2**, **3** and **4** as well as in the related Fe(III) compounds.<sup>[10-11]</sup> In particular, two extra sets of  $\pi$ - $\pi$  and P4AE interactions (in 2D and 3D) that are solely observed in **2** and **3** are believed to be responsible for the high spin-transition temperature in the compounds. That is because these interactions enhance the surface area between adjacent Fe(II) molecules and develop the propagation of spin crossover throughout the material.<sup>[27]</sup>

In searching for trends,  $\pi$ - $\pi$  interactions have been shown to influence the very high  $T_{1/2}$  temperature in the heteroleptic complex [Fe(3-MeOSalEen)(thsa)].<sup>[24a]</sup> In the [Fe(qsal-X)<sub>2</sub>] case,  $\pi$ - $\pi$  interactions in **2**, **3** and **4** are comparable, thus the relationship between  $\pi$ - $\pi$  interactions and the  $T_{1/2}$  temperature in the compounds is unclear. This might be either due to the smaller difference in  $T_{1/2}$  among [Fe(qsal-X)<sub>2</sub>] compounds compared to the review in the [Fe(3-MeOSalEen)(thsa)]<sup>[24a]</sup> work or it is due to the smaller effect of  $\pi$ - $\pi$  interactions on  $T_{1/2}$  in the [Fe(qsal-X)<sub>2</sub>] system. On the other hand, there is a trend in the P4AE interactions among compound **2**, **3** and **4**. It is interesting to note that P4AE interactions are weaker from X = I < Cl < Br as the  $T_{1/2}$  increases. This observation does not seem plausible as the molecules connecting through weaker interactions would require higher energy to propagate spin transition throughout

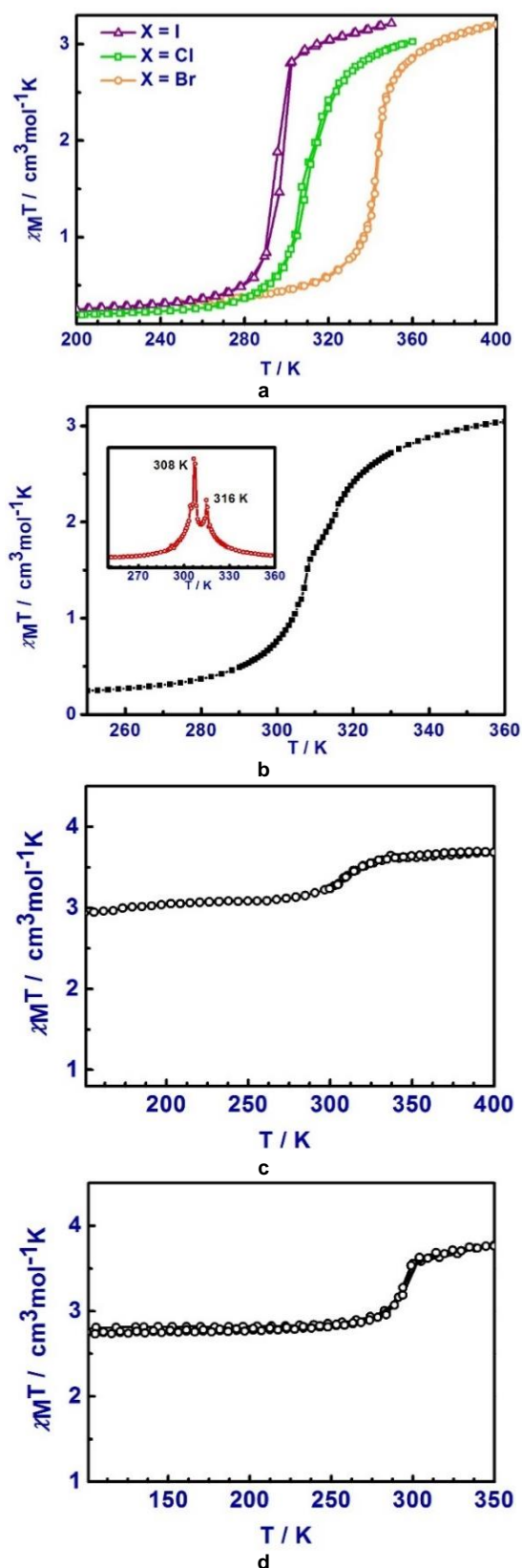


**Figure 5** Variable-temperature magnetic susceptibility ( $\chi_M T$ ) measurements for compound a) **2**, **3** and **4**, b) **2** with more steps, an inset shows the first order differentiation of the magnetic plot c) mixture of **2** and **2'** and d) mixture of **4** and **4'** from the 2 week reactions. Fig. 5b reproduced from ref. 7 with permission of the Royal Society of Chemistry.

the system, thus resulting in higher spin transition temperature. However, this might be a system specific effect.

For the 'two week' syntheses of **2** and **4**, a mixture of HS Fe(III) (**2'** and **4'**) and the SCO Fe(II) compounds were sometimes formed. In the case of **2+2'**, the  $\chi_M T$  value of about  $3 \text{ cm}^3 \text{ K mol}^{-1}$  at 100 K increases a little up to 300 K. After that it suddenly jumps to the  $\chi_M T$  value of  $3.52 \text{ cm}^3 \text{ K mol}^{-1}$  at 320 K then reaches a value of  $3.68 \text{ cm}^3 \text{ K mol}^{-1}$  at 400 K. A similar profile is observed in the mixture of **4+4'** but the magnetic susceptibility is slightly lower at intermediate temperature ( $2.8 \text{ cm}^3 \text{ K mol}^{-1}$  at 100 K) and approaches a more HS value at high temperature ( $3.77 \text{ cm}^3 \text{ K mol}^{-1}$  at 350 K). The slight differences in magnetic susceptibilities between **2+2'** and **4+4'** are possibly either from the intrinsic nature of the compounds or different mixture ratio between Fe(II)/Fe(III). The spin transitions noted in the mixtures correspond to the spin crossover of the Fe(II) components and take place at the same temperatures as in the pure Fe(II) compounds.

#### Powder diffraction data

To confirm the presence of Fe(II)/Fe(III) mixture in the 'two week' reaction media leading to **2** and **4**, PXRD experiments have been performed at room temperature. PXRD results after 1 week and 2 week reactions were examined in comparison to the simulated PXRD patterns calculated from the single crystal data of related Fe(II) and Fe(III) compounds. In Figure 6, the results for the 1 week samples of **2** and **4** agree well with the simulated PXRD pattern of Fe(II) and indicate the presence of a single phase in bulk samples. After 2 weeks, the overall pattern of such samples are similar to those for the 1 week sample as they both contain the Fe(II) compounds. However, the 2 weeks sample shows some particular peaks belonging to the Fe(III) components, indicative of a mixture of products. For **2+2'**, there are two extra peaks having  $2\theta$  ca.  $8^\circ$  and  $10^\circ$  assigned to (0,1,0), (0,1,1) and (1,0,1), (1,1,0) planes and belong to a new phase, namely **2'**. In the same way, there is one extra peak at  $2\theta = 25.5^\circ$  observed in the mixture of **4+4'** which corresponds to **4'** confirming the existence of both Fe(II) and Fe(III) compounds in these long time reactions. The stability of Fe(II) complexes in solution, at room temperature, has been studied by cyclic voltammetry and EPR spectroscopy confirming that oxidation of Fe(II) to Fe(III) occurs (Figure S8)

**Table 3** A review of Fe(II) compounds with N<sub>2</sub>O tridentate ligands illustrating their thermal and LIESST SCO properties

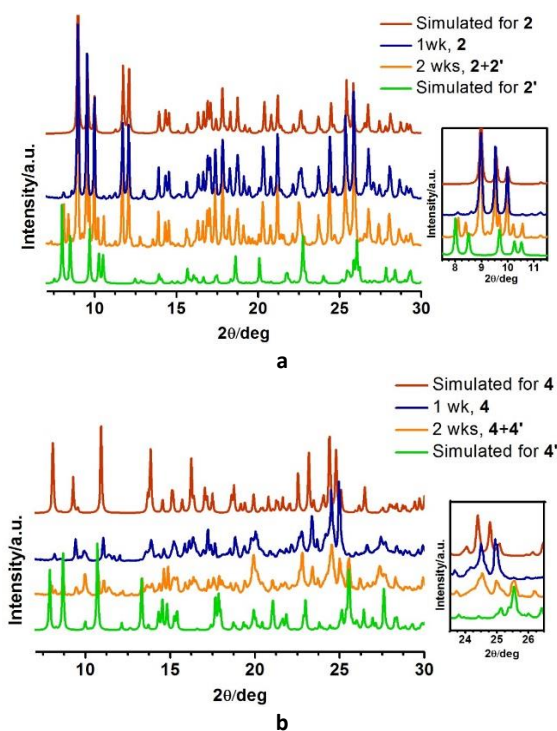
Complexes <sup>a</sup>	SCO	T <sub>1/2</sub> /K <sup>b</sup>	ΔT/K <sup>c</sup>	% HS,(LIESST)	Ref
Fe(L) <sub>2</sub> ·CH <sub>3</sub> OH	Abrupt	340	60		[14a]
Fe(L) <sub>2</sub>	Abrupt	285	7	58% <sup>d</sup> , 74 K	[14a]
[Fe(qnal) <sub>2</sub> ].CH <sub>2</sub> Cl <sub>2</sub>	Abrupt	220		≈79% <sup>e</sup> , 71 K	[14b]
[Fe(qnal) <sub>2</sub> ]	Abrupt	265		≈40% <sup>e</sup> , 57 K	[14b]
[Fe(Hqsalc) <sub>2</sub> ]	Abrupt	150	21		[15]
[Fe(qnal-12) <sub>2</sub> ].2C <sub>6</sub> H <sub>6</sub>	HS				[15]
Fe(pap-5NO <sub>2</sub> ) <sub>2</sub>	Abrupt	308	17	≈48% <sup>f</sup> , 58 K	[5]
Fe(qsal-5NO <sub>2</sub> ) <sub>2</sub>	Gradual incomplete				[5]
[Fe(L <sup>2</sup> ) <sub>2</sub> ](OTf) <sub>2</sub>	HS				[28]
Fe(L <sup>1</sup> ) <sub>2</sub>	HS				[23a]
Fe(L <sup>2</sup> ) <sub>2</sub>	Gradual incomplete			2% <sup>g</sup> , 43 K	[23a]
Fe(L <sup>3</sup> ) <sub>2</sub>	Mainly LS				[23a]
Fe(L <sup>4</sup> ) <sub>2</sub>	Two step incomplete			75% <sup>g</sup> , 76 K	[23a]
Fe(L <sup>5</sup> ) <sub>2</sub>	Gradual			35% <sup>g</sup> , 57 K	[23a]
Fe(L <sup>6</sup> ) <sub>2</sub>	Mainly LS				[23a]
Fe(L1) <sub>2</sub>	Gradual	243	3	87% <sup>g</sup> , 36 K	[23b]
Fe(L2) <sub>2</sub>	Gradual incomplete	~330			[23b]

Note <sup>a</sup> These are only mononuclear Fe(II) complexes with N<sub>2</sub>O tridentate ligand donors., <sup>b</sup> T<sub>1/2</sub> for heating mode, <sup>c</sup> hysteresis width for complete SCO, <sup>d</sup> 660 nm light irradiation, <sup>e</sup> 550 nm light irradiation, <sup>f</sup> 750 nm light irradiation <sup>g</sup> 532 nm light irradiation, <sup>h</sup> 650 nm light irradiation, <sup>i</sup> 640 nm light irradiation, <sup>14a</sup>L = 4-hydroxy-N-((pyridin-2-yl)-methylene)-benzohydrazide<sup>15</sup>Hqnal-12 = N-(8-quinolyl)-1-hydroxy-2-naphthalidimide, H<sub>2</sub>qsalc = 4-hydroxy-3-[(8-quinolinylimino)methyl]benzoic acid<sup>28</sup>L<sup>2</sup> = 4-[[6-methanol)-2-pyridyl]-3-aza-3-butenyl]<sup>23a</sup>HL<sup>1</sup> = N-((pyridin-2-yl)methylene)benzohydrazide, HL<sup>2</sup> = N-(1-(pyridin-2-yl)ethylidene)-benzohydrazide, HL<sup>3</sup> = N-(phenyl(pyridin-2-yl)methylene)benzohydrazide, HL<sup>4</sup> = 2-hydroxy-N-((pyridin-2-yl)methylene)benzohydrazide, HL<sup>5</sup> = 2-hydroxy-N-(1-(pyridin-2-yl)ethylidene)benzohydrazide, HL<sup>6</sup> = 2-hydroxy-N-(phenyl(pyridin-2-yl)methylene)benzohydrazide, <sup>23b</sup>HL1 = 2-hydroxy-3-methyl-N-[1-(pyridine-2-yl)-butylidene]benzohydrazideHL2 = 2-hydroxy-N-[1-(pyridine-2-yl)butylidene]benzohydrazide

**Table 4** Comparison of SCO properties and intermolecular interactions found in the present and related compounds

compound	Ref [11]	Ref [10]	1	2	3	4
SCO	Abrupt, 2-steps	Abrupt	HS	Abrupt, 2-steps	Abrupt	Abrupt
T <sub>1/2</sub> /K	136, 232	228		308, 316	342	295
Note	symmetry breaking		symmetry breaking			
<b>Interactions</b>						
In 1D	2(π-π), C-H...O	2(π-π), C-H...O	π-π	2(π-π), C-H...O	2(π-π), C-H...O	2(π-π), C-H...O
In 2D	C-H...Br		C-F...O, C-H...O	2(π-π)	C-H...Br, 2(π-π)	I...π
In 3D	P4AE	P4AE	C-H...F	2(P4AE), C-H...Cl	2(P4AE), C-H...Br	P4AE, I...π

Ref [11] = [Fe<sup>II</sup>(qsal-Br)<sub>2</sub>]NO<sub>3</sub>·2MeOH, Ref [10] = [Fe<sup>II</sup>(qsal-I)<sub>2</sub>]CF<sub>3</sub>SO<sub>3</sub>·MeOH, Interactions involving solvents and anions are omitted

**Figure 6** Comparison of PXRD patterns between simulated PXRD of Fe(II) and Fe(III) complexes and experimental PXRD patterns for the 1 week and 2 weeks sample for a) 2 and b) 4

### Photomagnetic LIESST results

The effect of light irradiation on compounds **2**, **3** and **4** was also studied. For all of them, irradiations at 405, 510, 650, 830 and 980 nm were tested and a 650 nm irradiation induced the most efficient photoconversion. For all of them the  $T(\text{LIESST})$  curve was recorded (Figure 7 **Fehler! Verweisquelle konnte nicht gefunden werden.**)<sup>[29]</sup> This curve, recorded at a constant temperature scan rate of 0.4 K/min, yields information on the lifetime of the photo-induced metastable state. The relaxation temperature  $T(\text{LIESST})$  is obtained by measuring the minimum of the  $\delta\chi_M T/\delta T$  curve. A common feature to **2**, **3** and **4** is the shape of the  $T(\text{LIESST})$  curve. Increasing the temperature from 10 K in the dark, after photo-saturation was reached, induces an increase of the  $\chi_M T$  value. This usually follows from the Fe(II) zero-field splitting.<sup>[30]</sup> After a maximum in the  $T(\text{LIESST})$  curve, the  $\chi_M T$  value drops down to the base line.

Regarding the photoconversion efficiency, long photoexcitation times are needed (more than 3 hours) and it increases from less than 15 % for **3**, to 30 % for **2** and 90 % in **4**. It is noteworthy that, for **4**, this is the highest conversion to the HS form by light that has been reported for Fe(II) with N<sub>2</sub>O tridentate ligands (see **Fehler! Verweisquelle konnte nicht gefunden werden.**). The  $T(\text{LIESST})$  value follows the

same trend according to **3** (30 K) < **2** (40 K) < **4** (54 K). These trends for **2**, **3** and **4** agree with the inverse energy gap law introduced by Hauser and the T(LIESST) vs  $T_{1/2}$  database that predicts that the compounds with higher thermal  $T_{1/2}$  tend to show poorer LIESST results.<sup>[29a]</sup>

Because of the small photoconversion efficiency in **2** and **3**, relaxation kinetics were recorded only in the case of compound **4** (insert **Fehler! Verweisquelle konnte nicht gefunden werden**. Figure 7c). The relaxation curves are very slightly sigmoidal, with a small exponential relaxation at short time scale. To extract the relaxation rate constant at each temperature, we have considered a self-accelerated law.<sup>[31]</sup> The insert of Figure 7c reports the simulations of the kinetics obtained with this approach. The thermodynamic parameters  $E_a$  (550  $\text{cm}^{-1}$ ),  $k^\infty$  ( $1.5 \cdot 10^3 \text{ s}^{-1}$ ) and  $E_a^*$  ( $\sim 55 \text{ cm}^{-1}$ ) were extracted from the Arrhenius plot ( $\ln k_{\text{HL}}$  vs  $1/T$ , insert Figure 7c).  $E_a$  is the activation energy,  $k^\infty$  the pre-exponential factor,  $k_{\text{HL}}$  the relaxation rate.

### Mössbauer spectroscopic studies

The samples used were the same as those used for magnetic studies and were made as described above, without any protective coating and in unsealed, custom built Teflon containers. The  $^{57}\text{Fe}$  Mössbauer spectra of the compounds were performed at low ( $\sim 5 \text{ K}$ ) and room temperatures to confirm the presence of LS and HS forms. The spectral parameters of the compounds are shown in Table 5 and Figure S10. The results are typical for Fe(II) complexes with quadrupole splitting,  $\Delta E_Q$ , and isomer shift,  $\delta$  of ca. 1 and 0.5  $\text{mm s}^{-1}$  for LS forms while they are about 2 and 1  $\text{mm s}^{-1}$  for HS forms, respectively.<sup>[3c, 32]</sup> For compound **2**<sup>[7]</sup> and **4**, the fully Fe(II) LS forms exist at low temperatures. At room temperature, some fractions of Fe(II) HS are also present. In the case of **3**, only fully LS forms are observed up to RT. These Mössbauer data correspond well with the magnetic results confirming exceptionally high  $T_{1/2}$  in the compounds. Unfortunately, we cannot get the fully HS Fe(II) Table 5  $^{57}\text{Fe}$  Mössbauer spectral parameters for **2**, **3** and **4**

results at such high a temperature from our Mössbauer facility.

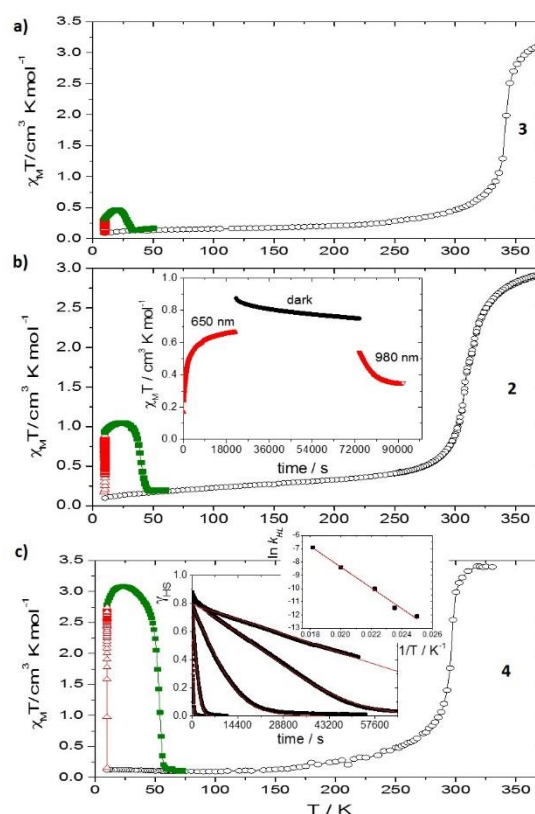


**Figure 7** Behaviour of the  $\chi_M T$  values for **3** (a), **2** (b) and **4** (c) in the dark (o), under a 650 nm irradiation ( $\Delta$ ) and after this irradiation in the dark at 0.4 K/mn ( $\blacksquare$ ). The insert of b) reports the time dependence of the  $\chi_M T$  values in **2** following irradiation at 650 nm ( $\blacktriangle$ ) and 980 nm ( $\blacktriangledown$ ) compared to the relaxation in the dark at 10 K ( $\blacksquare$ ). The insert of c) reports the different relaxation kinetics recorded as a function of the time for **4** (at 40, 42.5, 45, 50 and 55 K). The red lines stand for the fits discussed in the text. The second insert presents the Arrhenius plot with the straight line fit. Fig. 7b reproduced from ref. 7 with permission of the Royal Society of Chemistry.

Compound	T (K)	Spin State	$\delta$ (mm/s)	$\Delta E_Q$ (mm/s)	$\Gamma_{LR}$ (mm/s)	I (%)
<b>2</b> <sup>[7]</sup>	5.9	LS	0.43	1.09	0.27/0.24	100
	295	LS	0.34	1.03	0.36	90
		HS	1.20 <sup>a</sup>	1.87	0.27/0.65	10
<b>3</b>	5.6	LS	0.42	1.08	0.28/0.25	100
	293	LS	0.35	1.04	0.32/0.27	100
<b>4</b>	5.4	LS	0.42	1.02	0.26/0.25	100
	293	LS	0.34	1.00	0.35	85
		HS	1.17	1.99	0.35	15

<sup>a</sup> Strong evidence for HS Fe(II) but unable to fit unambiguously.

## DSC results

Differential scanning calorimetry (DSC) data were collected on compound **2**, **3** and **4** using a 10 K min<sup>-1</sup> scan rate. From the DSC plots in Figure S11 and Table S9, for **2**<sup>[7]</sup>, there are two peaks for endo- and exothermic measurements while there is only one peak shown in the cases of **3** and **4**, with a weak shoulder on the endothermic sweep for **4**, at ~295 K. All the phase transition temperatures from the DSC data are in the same ranges as the spin transition results from magnetic measurements. As mentioned above, the initial magnetic plot for **2** roughly suggested a one-step SCO with an abrupt spin transition. The DSC result confirms the two step SCO present in this compound. Moreover, the small  $\Delta S$  value of 19.8 J/mol K in **2**, compared to those in **3** and **4**, being a factor of two lower than in the iso-structural compound **3**, agrees with data by Wang and Gao *et al.* who also reported that symmetry breaking associated with a two-step SCO led to a significant lowering in  $\Delta H$  and  $\Delta S$  values.<sup>[20]</sup> The weak shoulder noted for **4** might relate to CH<sub>2</sub>Cl<sub>2</sub> desolvation effects but we have no evidence for this, with the  $\chi_M T$  plot not showing any related inflection.

## Theoretical studies

Density Functional Theory (DFT) calculations have been undertaken using hybrid B3LYP functional (see computational details) to rationalise the spin-crossover features observed in the monomeric Fe(II) complexes **2-4** and the Fe(III) analogue **4'**. We have optimized the complexes **2-4** in their respective high spin (HS,  $t_{2g}^4 e_g^2$ ), intermediate spin (IS,  $t_{2g}^5 e_g^1$ ) and low spin (LS,  $t_{2g}^6 e_g^0$ ) ground states and also for complex **4'** with its respective high spin ( $t_{2g}^3 e_g^2$ ), intermediate spin ( $t_{2g}^4 e_g^1$ ) and low spin ( $t_{2g}^5 e_g^0$ ) states using the X-ray structural coordinates as input data. The geometry optimizations are all performed in the gas phase. Optimized structural parameters for **2-4** and **4'** along with X-ray structural parameters at 100 K are summarised in Table S10 and are in good agreement.

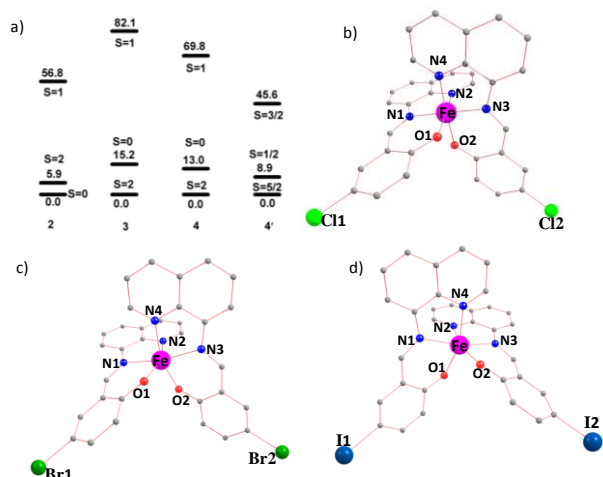


**Figure 8** a) Energy level gaps (in kJ mol<sup>-1</sup>) computed for different electronic configurations in **2-4** and **4'**. Optimized ground state structure of b) **2** (LS) c) **3** (HS) and d) **4** (HS).

The computed energies of complexes **2-4** and **4'** and the optimised ground state structures of **2-4** are shown in Figure 8. Calculations predict a LS ground state for complex **2** and high-spin for **3**, **4** and **4'**. The LS predicted

for complex **2** and HS predicted for **4'** are consistent with the experimental observations, however HS ground states predicted for complexes **3** and **4** are at odds with experiment. Although the ground state predictions are contradicting experiments for these two complexes,<sup>[33]</sup> the high-spin (HS) state and the low-spin (LS) state gaps are estimated to be very small for all complexes (5.9 kJ mol<sup>-1</sup>, 15.2 kJ mol<sup>-1</sup> and 13.0 kJ mol<sup>-1</sup> and 8.9 kJ mol<sup>-1</sup> for complexes **2**, **3**, **4** and **4'**, respectively). These small gaps lie within the range expected for the observation of SCO behaviour as witnessed in the experiments.<sup>[34]</sup> However, the small gap prediction of **4'** is inconsistent with the solid state experimental results mentioned above. This contradiction suggests that the calculations in the gas phase, without intermolecular interactions included, are not sufficient to predict SCO behavior in this compound. Intermolecular and lattice effects are known to significantly influence the spin state energetics and the predicted  $\Delta E(\text{HS-LS})$  gaps are small for all complexes.<sup>[5, 35]</sup> Recently, an elastic model with elastic frustration in the lattice has been reported and claimed to be a good description for two-step spin crossover.<sup>[36]</sup> Incorporation of such effects might improve the present computed results. The intermediate-spin (IS) states lie much higher in energy for all complexes. This is essentially due to the fact that to achieve the IS spin state, the  $(d_{xy})^2(d_{yz})^2(d_{xz})^1(d_z^2)^1$  configuration is required and this suggests breaking the  $\pi$  orbital symmetry of the  $d_{xz}$ ,  $d_{yz}$  orbital leading to a large spin pairing energy and high lying  $S = 1$  state.

To probe the nature of iron-ligand bonding, we have plotted the energies of d-based orbitals of **2-4** computed in the gas phase are shown in Figure 9 and Figure S12. DFT calculations yield the following Fe(II) electronic configuration  $(d_{xy})^2(d_{xz})^1(d_{yz})^1(d_{x^2-y^2})^1(d_z^2)^1$  for **2-4** and  $(d_{xz})^1(d_{yz})^1(d_{xy})^1(d_{x^2-y^2})^1(d_z^2)^1$  for Fe(III) **4'**, in the high-spin configurations. The energy gap between the  $t_{2g}$ -like and  $e_g$ -like orbitals are estimated to be 96.9, 195.1, and 188 kJ mol<sup>-1</sup> for complexes **2-4** respectively. A large gap suggests stabilization of the LS ground state for these complexes, as observed. The  $d_z^2$  orbital is found to be along the N-Fe-N axis while the  $d_{x^2-y^2}$  orbital found to lie in the N<sub>2</sub>O<sub>2</sub> equatorial plane. Although the presence of the oxygen atoms enhance the electrostatic interaction in the equatorial plane with relatively shorter bond lengths (Fe-O vs. Fe-N), the equatorial plane is significantly distorted (twist angle between N-Fe-N and O-Fe-O plane is ~27°) leading to weaker Fe-N bonds. For this reason the  $d_z^2$  and  $d_{x^2-y^2}$  orbitals are found to be nearly degenerate for all three complexes **2-4**.

The presence of halogen atoms in the qsal ligand promote stronger delocalization and particularly perturbs the energies of the  $d_{xz}$  and  $d_{yz}$  orbitals as we move along the -Cl to -I substitution. As -Cl is a stronger  $\pi$  donor ligand compared to -Br or -I, the  $d_{xz}$  and  $d_{yz}$  orbitals in the case of -Cl are strongly destabilized compared to -Br and -I leading to a smaller  $t_{2g}-e_g$  gap. As the SCO properties are correlated to the crystal field splitting and also the pairing

energy, very strong anti-bonding interactions observed for the -Cl derivative (See Figure S12) also enhances the pairing energy compared to -Br and -I analogues and this compensates the lower  $t_{2g}$ - $e_g$  gap estimated for -Cl leading to the observation of SCO at relatively higher temperature.

Computed spin density plots for the HS state for complexes **2**, **3** and **4** are shown in Figure 10. The Fe(II) centres of complexes **2** and **4** possess a spin density of 3.82 while complex **3** has a slightly higher value (3.85). This suggests stronger delocalization of spin densities for complexes **2** and **4** and a relatively localized picture for complex **3**. This is also reflected in the spin density distribution observed on the donor atoms where, particularly, the two nitrogen atoms in the axial direction possess a spin density of  $\sim 0.03$  for complexes **2** and **4** while in complex **3** these nitrogen atoms possess spin density of  $\sim 0.07$  revealing significant spin delocalization due to  $d_{z^2}$  orbitals.

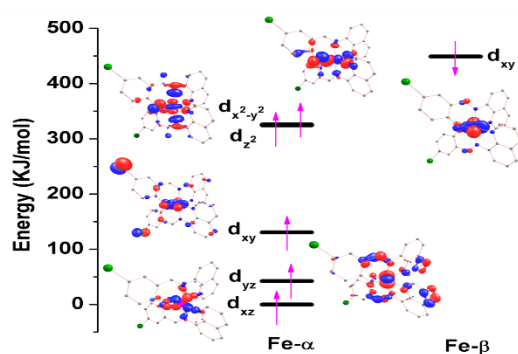


Figure 9 Eigenvalue plot computed for complex **3**

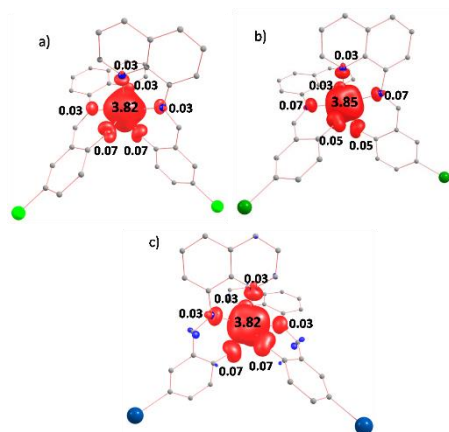


Figure 10 B3LYP computed spin density plots of the HS state for a) complex **2** b) complex **3** and c) complex **4**.

## Conclusions

The family of Fe(II) complexes  $[\text{Fe}^{\text{II}}(\text{qsal-X})_2]$  where X = F, Cl, Br and I, has provided an unprecedented array of magnetic and spin crossover properties.  $[\text{Fe}(\text{qsal-Cl})_2]$  is the first Fe(II) compound with a  $\text{N}_2\text{O}$  donors that exhibits symmetry breaking accompanied by a two-step SCO above room temperature, the highest temperatures reported thus

far for symmetry breaking mononuclear SCO compounds (viz.  $T_{1/2} = 308$  and 316 K).  $[\text{Fe}(\text{qsal-Br})_2]$  shows thermal SCO at the highest spin transition temperature reported in the qsal<sup>1</sup> ligand families and in any other Fe(II)- $\text{N}_2\text{O}$  tridentate ligand system ( $T_{1/2} = 342$  K).  $[\text{Fe}(\text{qsal-I})_2]\text{CH}_2\text{Cl}_2$  exhibits an abrupt thermal spin transition at ambient temperature ( $T_{1/2} = 295$  K) and almost fully HS conversion upon photoirradiation ( $T(\text{LIESST}) = 54$  K). Uniquely for this halogen-substituted ligand family,  $[\text{Fe}(\text{qsal-F})_2]$  does not show spin crossover but remains HS between 2 and 360 K.

In regard to halogen substituent effects,  $[\text{Fe}(\text{qsal-F})_2]$  exhibits a distinct supramolecular structure as well as the HS magnetic properties (*vide supra*). The oxidation states of the metal centre ( $\text{Fe}^{\text{II}}/\text{Fe}^{\text{III}}$ ) and the presence of anions in the structures ( $\text{Fe}^{\text{III}}$ ) significantly impact the crystal packing and magnetic properties in the complexes. On the other hand, the other  $[\text{Fe}^{\text{II}}(\text{qsal-X})_2]$  complexes still maintain the Fe-qsal characters. Cl and Br substituents prefer to form C-H $\cdots$ X interactions while I $\cdots\pi$  interaction is the preference for the I-substituted case. Consequently, the two extra sets of  $\pi$ - $\pi$  and P4AE interactions, seen in Cl and Br substituents, are absent in  $[\text{Fe}^{\text{II}}(\text{qsal-I})_2]$ . This is because I $\cdots\pi$  interactions dictate the packing of the  $[\text{Fe}^{\text{II}}(\text{qsal-I})_2]$  moieties and prevent two extra sets of  $\pi$ - $\pi$  and P4AE interactions from forming. This possibly results in the lowest  $T_{1/2}$  value comparing to compound **2** and **3**. For an isostructural pair, X = Cl (**2**) and Br (**3**), the absence of C2-H2 $\cdots$ Cl1 interaction is suggested to be responsible for slightly weaker cooperativity in  $[\text{Fe}^{\text{II}}(\text{qsal-Cl})_2]$ .

In general, the  $[\text{Fe}^{\text{II}}(\text{qsal-X})_2]$  complexes, where X = Cl, Br and I, exhibit an abrupt SCO at a high temperature in comparison to Fe(III) analogues  $[\text{Fe}^{\text{III}}(\text{qsal-X})_2]\text{Y}$ . We propose that this is due to an absence of anions/solvents in the lattice that allow the Fe(II) molecules to have larger surface contact (*via* two extra sets of  $\pi$ - $\pi$  and P4AE interactions for **2** and **3**, I $\cdots\pi$  interaction for **4**) than for the Fe(III) complexes which enhances the strong cooperativity. Subsequently, to design a potential spin crossover material, the fundamental requirements for an abrupt spin crossover, particularly in Fe-qsal complexes, is the combination of the symmetrical two sets of  $\pi$ - $\pi$  and P4AE interactions. To show spin transition at exceptionally high temperatures, the extra two sets of  $\pi$ - $\pi$  and P4AE interactions are further recommended.

In order to try and quantify some of the above qualitative observations and correlations, DFT calculations were carried out on complexes **2-4** and **4'** to elucidate their electronic structures and to rationalize the origin of SCO features and thermodynamic properties. We were aware of the limitations of DFT in predicting spin state energies and SCO in iron(II) systems, described by Neese and coworkers.<sup>[33a]</sup> Although the complexes have  $\text{N}_4\text{O}_2$  coordination environments where oxygen atoms form rather strong Fe-O bonds, the presence of two oxygen atoms in a *cis* arrangement in the equatorial plane leads to significant distortions and the strong Fe-O bonds are compensated by the relatively large Fe-N bonds in the LS configurations.

This reduces the strong  $\sigma$ -antibonding interactions thus leading to lower HS-LS gaps. The presence of  $\pi$ -donor halogen atoms in the qsal ligands are found to influence the energies of  $d_{xz}/d_{yz}$  orbitals leading to variation in the  $T_{1/2}$  values for complexes **2-4**. The computed parameters are in general agreement with the experimental observations, although there are discrepancies in fine detail such as ground state energies, possibly due to a lack of inclusion of an elastic model, referred to above,<sup>[36]</sup> and/or inclusion of intermolecular interactions such as Madelung potential fields, recently used in calculations on solid state Fe(II) spin crossover systems.<sup>[37]</sup>

## Experimental Section

**General:** All reagents and solvents were purchased from Sigma–Aldrich and used as received. Infrared spectra were measured with a Bruker Equinox 55 FTIR spectrometer fitted with a 71Judson MCT detector and Specac Golden Gate diamond ATR. Mass spectrometry analyses were performed using electrospray ionization mass spectra (ESI-MS) and were recorded with a Micromass (now Waters) ZMD with Waters alliance e2695 HPLC system for automatic sample injections. MeOH was the mobile phase and had a flow rate of 100  $\mu\text{L min}^{-1}$ . TGA measurements were performed using a MettlerTGA/DSC 1 thermal analysis instrument at a heating rate of 2  $^{\circ}\text{C min}^{-1}$ . Microanalyses were performed by Campbell Microanalytical Laboratory, Department of Chemistry, University of Otago, Dunedin, New Zealand. Variable-temperature magnetic susceptibility data were collected using either a Quantum Design MPMS 5 superconducting quantum interference device (SQUID) magnetometer or a MPMS XL-7 SQUID magnetometer, with a scan speed of 10  $\text{K min}^{-1}$  followed by a one minute wait after each temperature change. In cases in which steps were less than 10 K the target temperature was reached in less than 1 min; hence it takes longer to stabilise at the target temperature. X-ray powder diffraction patterns recorded with a Bruker D8 Advance powder diffractometer operating at Cu  $K\alpha$  wavelength (1.5418 Å), with samples mounted on a zero-background silicon single crystal stage. Scans were performed at room temperature in the  $2\theta$  range 5–55 $^{\circ}$ .

Mössbauer spectra were recorded on a spectrometer from SEE Co. (Science Engineering & Education Co., MN) equipped with a closed cycle refrigerator system from Janis Research Co. and SHI (Sumitomo Heavy Industries Ltd.). Data were collected in constant acceleration mode in transmission geometry. The zero velocity of the Mössbauer spectra refers to the centroid of the room temperature spectrum of a 25  $\mu\text{m}$  metallic iron foil. Analysis of the spectra was conducted using the WMOSS program (SEE Co, formerly WEB Research Co. Edina, MN).

X-ray crystallographic measurements on **1** and **2'** were collected at 123 K using a Bruker Smart Apex X8 diffractometer with Mo- $K\alpha$  radiation ( $\lambda = 0.71073$  Å). Single crystals were mounted on a glass fibre using oil. The data collection and integration were performed within SMART and SAINT+ software programs and corrected for absorption using the Bruker SADABS program.<sup>[38]</sup>

X-ray crystallographic measurements on **2**, **3** and **4** were collected at the Australian Synchrotron operating at approximately 16 keV ( $\lambda$

= 0.71073 Å). The collection temperature was maintained at specified temperatures using an open-flow  $\text{N}_2$  cryostream. Data were collected using Blue Ice software.<sup>[39]</sup> Initial data processing was carried out using the XDS package.<sup>[40]</sup>

X-ray crystallographic measurements on **2** and **3** were collected at the University of Canterbury on an Agilent Supernova dual source (Cu, Mo) diffractometer fitted with an Atlas detector. For **2**, the crystal quality was checked at 298 K by mounting on a loop with paratone oil, then the oil manually removed and the crystal remounted on a glass fibre with a minimal amount of epoxy resin. Full collections were performed at 298 K, 312 K, 330 K, 308 K, 318 K and 100 K in that order, with a ramp rate of 60  $\text{K h}^{-1}$  (1  $\text{K min}^{-1}$ ) for all changes of the temperature (with the exception of 298 K to 100 K, where 120  $\text{K h}^{-1}$  (2  $\text{K min}^{-1}$ ) was used). A relaxation period of 15 minutes (from the time the final temperature was reached) for each temperature studied was allowed. Collection of complete data required approximately 24 hours per sample. After the six full collections (and numerous unit cell studies), no degradation of the crystal was observed, either physically or experimentally. All collections were performed with 20/80 (inner/outer data) second exposure times (correlated frames, so effectively 10/40 second exposures) for consistency.

For **3**, a crystal was mounted using a cryo-oil and its quality assessed at 120 K. A suitable crystal was transferred and the oil manually removed. The crystal was mounted on a glass fibre using superglue (capable of surviving the high temperatures without degradation) and heated to 380 K with a ramp rate of 300  $\text{K h}^{-1}$  (5  $\text{K min}^{-1}$ ) to the final temperature. An additional unit cell study was performed mid-transition at 330 K, however, this proved inconclusive. Once at the target temperature, the crystal was left to settle for 15 min and then unit cell studies were performed (30-60 min). Collection of complete data required 48-72 hours per sample. Data reduction was performed with CrysAlis Pro (Agilent Technologies, 2013) and refinement with the Olex2 (Dolomanov et al., 2009) software. CCDC numbers 1495806-1495818. These data are provided free of charge by The Cambridge Crystallographic Data Centre.

Photomagnetic measurements were performed using a 650 nm photo-diode coupled by means of an optical fibre to the cavity of a MPMS-5S Quantum Design SQUID magnetometer. The optical power at the sample surface was adjusted to prevent important warming of the sample. The compound consists of a thin layer. Its weight was obtained by comparison of the thermal spin crossover curve with that of a more accurately weighted sample of the same material. Our previously published standardized method for measuring LIESST data was followed<sup>[29b]</sup>: After being slowly cooled at 10K, the sample in the low-spin state was irradiated and the change in magnetic susceptibility was followed. When the saturation point was reached the laser was switched off and the temperature increased at a rate of  $\sim 0.4$   $\text{K min}^{-1}$ . The magnetization was measured every 1 K.  $T(\text{LIESST})$  was determined from the minimum of a  $d\chi_M/dT$  vs.  $T$  plot for the relaxation process.

Cyclic voltammetric experiments were conducted using a conventional three electrode cell at  $293 \pm 2$  K with a CHI 700D electrochemical workstation (CH Instruments, Austin, Texas, USA). A 1 mm diameter glassy carbon (GC; EDAQ) working electrode was polished using an aqueous 0.3  $\mu\text{m}$  alumina slurry on a polishing

cloth (Buehler), rinsed with water, and then sonicated to remove residual alumina, rinsed with water again and then acetone. It was finally dried under N<sub>2</sub> before use. A 33 μm diameter carbon microelectrode (BAS; Japan) was polished using an aqueous 0.05 μm alumina slurry on a polishing cloth (Buehler), rinsed with water and acetone, and dried under N<sub>2</sub> before use. The reference electrode was a Ag wire quasi-reference, and its potential was calibrated against that of the ferrocene/ferricenium (Fc/Fc<sup>+</sup>) couple.

#### Computational details:

DFT<sup>[41]</sup> calculations have been performed on the X-ray structural coordinates of the complexes using the Gaussian 09 suite<sup>[42]</sup>. Calculations were performed in two steps i) optimizing the nuclear coordinates of the X-ray structure and ii) on top of the optimized coordinates frequency calculations have been performed to extract the thermodynamic parameters. All calculations employ Becke's exchange functional<sup>[43]</sup> together with correlation functional of Lee, Yang and Parr<sup>[44]</sup> (B3LYP as implemented in Gaussian) along with Ahlrichs polarised triple-ζ valence (TZVP)<sup>[45]</sup> basis set for the metal ion and for rest of the atoms. The frequency calculations are also performed using the B3LYP/TZVP level of theory and this has been shown to be superior in estimating thermodynamic quantities for spin crossover complexes.<sup>[35]</sup> Although B3LYP is known to have deficiency in reproducing correctly the spin ground state of Fe(II) SCO compounds,<sup>[34]</sup> systematic benchmarking by Jakubikova et al. reveals that the results are similar to those obtained from B3LYP\* and CASPT2 level of theory.<sup>[46,47,48]</sup>

#### Synthesis of ligands

Hqsal-X, where X = F, Cl, Br and I, were synthesized according to the literature method.<sup>[49]</sup>

#### Synthesis of complexes

Layered diffusion is the general procedure that has been used to prepare all of the complexes. For Fe(II) complexes: FeCl<sub>2</sub>·4H<sub>2</sub>O (40 mg, 0.2 mmol) was dissolved in MeOH (5 ml). The solution was stirred for 5 mins and then layered on to blank MeOH (3 ml). A solution of Hqsal-X (0.4 mmol) in CH<sub>2</sub>Cl<sub>2</sub> (2 ml) was in the bottom in which NEt<sub>3</sub> (56 μL, 0.4 mmol) had been added as a base. After 7 days, black crystals formed, were washed with hexane (2 x 1 ml) and acetone (2 x 1 ml) and then air dried. For **2'**, FeCl<sub>3</sub> (32 mg, 0.2 mmol) has been used instead of FeCl<sub>2</sub>·4H<sub>2</sub>O

[Fe(qsal-F)<sub>2</sub>] **1**; yield 28 mg (23%).  $\tilde{\nu}_{\max}/\text{cm}^{-1}$ : 3042 (ν<sub>Ar-H</sub>), 1597 (ν<sub>C=N</sub>), 1568 (ν<sub>C=C</sub>), 1230 (ν<sub>C-N</sub>). m/z (ESI) 586.0 [Fe(qsal-F)<sub>2</sub>]<sup>+</sup>. Calcd. for (found %) C<sub>32</sub>H<sub>20</sub>F<sub>2</sub>FeN<sub>4</sub>O<sub>2</sub>: C, 65.55 (65.25); H, 3.44 (3.42); N, 9.55% (9.51).

[Fe(qsal-Cl)<sub>2</sub>] **2**; yield 42 mg (34%).  $\tilde{\nu}_{\max}/\text{cm}^{-1}$ : 3043 (ν<sub>Ar-H</sub>), 1595 (ν<sub>C=N</sub>), 1562 (ν<sub>C=C</sub>), 1232 (ν<sub>C-N</sub>). m/z (ESI) 617.9 [Fe(qsal-Cl)<sub>2</sub>]<sup>+</sup>. Calcd. for (found %) C<sub>32</sub>H<sub>20</sub>Cl<sub>2</sub>FeN<sub>4</sub>O<sub>2</sub>: C, 62.06 (61.21); H, 3.26 (3.14); N, 9.05% (8.92).

[Fe(qsal-Cl)<sub>2</sub>]Cl·1.5MeOH·1.5H<sub>2</sub>O **2'**; yield 61 mg (42%).  $\tilde{\nu}_{\max}/\text{cm}^{-1}$ : 3041 (ν<sub>Ar-H</sub>), 1603 (ν<sub>C=N</sub>), 1522 (ν<sub>C=C</sub>), 1241 (ν<sub>C-N</sub>). m/z (ESI) 617.9 [Fe(qsal-Cl)<sub>2</sub>]<sup>+</sup>. Calcd. for (found %) C<sub>33.5</sub>H<sub>29</sub>Cl<sub>2</sub>FeN<sub>4</sub>O<sub>5</sub>: C, 55.13 (55.65); H, 4.00 (3.98); N, 7.68% (7.77); Cl, 14.57% (14.27).

[Fe(qsal-Br)<sub>2</sub>] **3**; yield 54 mg (38%).  $\tilde{\nu}_{\max}/\text{cm}^{-1}$ : 3046 (ν<sub>Ar-H</sub>), 1591 (ν<sub>C=N</sub>), 1565 (ν<sub>C=C</sub>), 1234 (ν<sub>C-N</sub>). m/z (ESI) 608.0 [Fe(qsal-Br)<sub>2</sub>]<sup>+</sup>. Calcd. for (found %) C<sub>32</sub>H<sub>20</sub>Br<sub>2</sub>FeN<sub>4</sub>O<sub>2</sub>: C, 54.27 (53.44); H, 2.85 (2.63); N, 7.91% (7.74).

[Fe(qsal-I)<sub>2</sub>]CH<sub>2</sub>Cl<sub>2</sub> **4**; yield 85 mg (48%).  $\tilde{\nu}_{\max}/\text{cm}^{-1}$ : 3044 (ν<sub>Ar-H</sub>), 1595 (ν<sub>C=N</sub>), 1559 (ν<sub>C=C</sub>), 1235 (ν<sub>C-N</sub>). m/z (ESI) 801.8 [Fe(qsal-

I)<sub>2</sub>]<sup>+</sup>. Calcd. for [Fe(qsal-I)<sub>2</sub>]·0.3CH<sub>2</sub>Cl<sub>2</sub> (found %) C<sub>32.03</sub>H<sub>20.06</sub>I<sub>2</sub>FeN<sub>4</sub>O<sub>2</sub>Cl<sub>0.6</sub>: C, 46.48 (47.05); H, 2.36 (2.44); N, 6.77 % (6.76). Partial de-solvation agrees with the crystal structure collected at room temperature.

## Acknowledgements

This work was supported by an Australian Research Council Discovery grant (to K.S.M.). Access to the Australian Synchrotron is gratefully acknowledged. PEK gratefully acknowledges the Royal Society of New Zealand Marsden Fund for financial support. We thank Professor David Harding (Walailak University) for valuable discussions, Dr. Si-Xuan Guo for help with electrochemistry studies and Mrs Sioe See Volaric (Melbourne University) for EPR assistance.

**Keywords:** spin crossover • Crystal structures • Fe(II) and Fe(III) complexes • intermolecular interactions • Schiff base ligands • halogen bonding

- [1] a) R. J. Deeth, C. M. Handley, B. J. Houghton, in *Spin-Crossover Materials* (Ed.: M. A. Halcrow), John Wiley & Sons Ltd, **2013**, 443-454; b) P. N. Martinho, C. Rajnak, M. Ruben, in *Spin-Crossover Materials* (Ed.: M. A. Halcrow), John Wiley & Sons Ltd, **2013**, 375-404; c) P. Gütllich, A. Hauser, H. Spiering, *Angew. Chem. Int. Ed. Engl.* **1994**, *33*, 2024-2054; d) A. Bousseksou, G. Molnar, L. Salmon, W. Nicolazzi, *Chem. Soc. Rev.* **2011**, *40*, 3313-3335; e) K. S. Murray, in *Spin-Crossover Materials* (Ed.: M. A. Halcrow), John Wiley & Sons Ltd, **2013**, 1-54; f) M. A. Halcrow, *Chem. Commun.* **2013**, *49*, 10890-10892.
- [2] a) M. Nihei, T. Shiga, Y. Maeda, H. Oshio, *Coord. Chem. Rev.* **2007**, *251*, 2606; b) P. Gütllich, H. A. Goodwin, in *Spin Crossover in Transition Metal Compounds I* (Eds.: P. Gütllich, H. A. Goodwin), Springer Berlin Heidelberg, Berlin, Heidelberg, **2004**, 1-47; c) B. Weber, E. Kaps, J. Weigand, C. Carbonera, J.-F. Létard, K. Achterhold, F. G. Parak, *Inorg. Chem.* **2008**, *47*, 487-496; d) B. Weber, W. Bauer, J. Obel, *Angew. Chem. Int. Ed.* **2008**, *47*, 10098-10101; e) S. Dorbes, L. Valade, J. A. Real, C. Faulmann, *Chem. Commun.* **2005**, 69-71; f) D. J. Harding, P. Harding, W. Phonsri, *Coord. Chem. Rev.* **2016**, *313*, 38-61; g) B. Weber, *Coord. Chem. Rev.* **2009**, *253*, 2432-2449.
- [3] a) M. Nihei, H. Tahira, N. Takahashi, Y. Otake, Y. Yamamura, K. Saito, H. Oshio, *J. Am. Chem. Soc.* **2010**, *132*, 3553-3560; b) T. D. Roberts, F. Tuna, T. L. Malkin, C. A. Kilner, M. A. Halcrow, *Chem. Sci.* **2012**, *3*, 349-354; c) P. Gütllich, Y. Garcia, H. A. Goodwin, *Chem. Soc. Rev.* **2000**, *29*, 419-427; d) R. Kulmaczewski, J. Olguín, J. A. Kitchen, H. L. C. Feltham, G. N. L. Jameson, J. L. Tallon, S. Brooker, *J. Am. Chem. Soc.* **2014**, *136*, 878-881; e) M. A. Halcrow, *Chem. Soc. Rev.* **2011**, *40*, 4119-4142.
- [4] B. Weber, E.-G. Jäger, *Eur. J. Inorg. Chem.* **2009**, *2009*, 465-477.
- [5] O. lasco, E. Rivière, R. Guillot, M. Buron-Le Cointe, J.-F. Meunier, A. Bousseksou, M.-L. Boillot, *Inorg. Chem.* **2015**, *54*, 1791-1799.
- [6] S. Hayami, Z.-z. Gu, H. Yoshiki, A. Fujishima, O. Sato, *J. Am. Chem. Soc.* **2001**, *123*, 11644-11650.
- [7] W. Phonsri, C. G. Davies, G. N. L. Jameson, B. Moubaraki, J. S. Ward, P. E. Kruger, G. Chastanet, K. S. Murray, *Chem. Commun.* **2017**. DOI 10.1039/C6CC10040F
- [8] a) K. Fukuroi, K. Takahashi, T. Mochida, T. Sakurai, H. Ohta, T. Yamamoto, Y. Einaga, H. Mori, *Inorg. Chem. Int. Ed.* **2014**, *53*, 1983-1986; b) N. Nassirinia, S. Amani, S. J. Teat, O. Roubeau, P. Gamez, *Chem. Commun.* **2014**, *50*, 1003-1005.
- [9] W. Phonsri, D. J. Harding, P. Harding, K. S. Murray, B. Moubaraki, I. A. Gass, J. D. Cashion, G. N. L. Jameson, H. Adams, *Dalton Trans.* **2014**, *43*, 17509-17518.
- [10] D. J. Harding, W. Phonsri, P. Harding, I. A. Gass, K. S. Murray, B. Moubaraki, J. D. Cashion, L. Liu, S. G. Telfer, *Chem. Commun.* **2013**, *49*, 6340-6342.
- [11] D. J. Harding, W. Phonsri, P. Harding, K. S. Murray, B. Moubaraki, G. N. L. Jameson, *Dalton Trans.* **2015**, *44*, 15079-15082.
- [12] a) D. Chernyshov, M. Hostettler, K. W. Törnroos, H.-B. Bürgi, *Angew. Chem. Int. Ed.* **2003**, *42*, 3825-3830; b) N. Bréfuel, H. Watanabe, L. Toupet, J. Come, N. Matsumoto, E. Collet, K. Tanaka, J.-P. Tuchagues, *Angew. Chem. Int. Ed.* **2009**, *48*, 9304-9307; c) Z.-Y. Li, J.-W. Dai, Y. Shiota, K. Yoshizawa, S. Kanegawa, O. Sato, *Chem. Eur. J.* **2013**, *19*, 12948-12952.

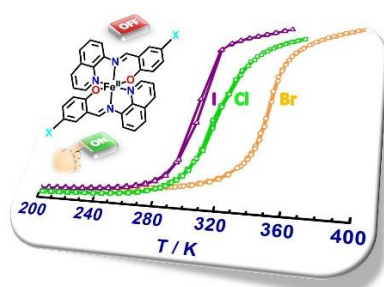
- [13] a) J. K. McCusker, A. L. Rheingold, D. N. Hendrickson, *Inorg. Chem.* **1996**, *35*, 2100-2112; b) M. Marchivie, P. Guionneau, J.-F. Letard, D. Chasseau, *Acta Crystallogr., Sect. B: Struct. Sci.* **2005**, *61*, 25-28.
- [14] a) L. Zhang, G.-C. Xu, H.-B. Xu, T. Zhang, Z.-M. Wang, M. Yuan, S. Gao, *Chem. Commun.* **2010**, *46*, 2554-2556; b) T. Kuroda-Sowa, Z. Yu, Y. Senzaki, K. Sugimoto, M. Maekawa, M. Munakata, S. Hayami, Y. Maeda, *Chem. Lett.* **2008**, *37*, 1216-1217.
- [15] T. Kuroda-Sowa, K. Kimura, J. Kawasaki, T. Okubo, M. Maekawa, *Polyhedron* **2011**, *30*, 3189-3192.
- [16] P. van Koningsbruggen, Y. Maeda, H. Oshio, in *Spin Crossover in Transition Metal Compounds I*, Vol. 233 (Eds.: P. Gütllich, H. A. Goodwin), Springer Berlin Heidelberg, **2004**, pp. 259-324.
- [17] W. Phonsri, *Ph. D. Thesis, Walailak University, Thailand* **2014**.
- [18] a) K. Takahashi, T. Sato, H. Mori, H. Tajima, O. Sato, *Phys. B* **2010**, *405*, S65-S68; b) D. Sertphon, D. J. Harding, P. Harding, K. S. Murray, B. Moubaraki, J. D. Cashion, H. Adams, *Eur. J. Inorg. Chem.* **2013**, *2013*, 788-795.
- [19] V. Russell, M. Scudder, I. Dance, *J. Chem. Soc., Dalton Trans.* **2001**, 789-799.
- [20] W. Zhang, F. Zhao, T. Liu, M. Yuan, Z.-M. Wang, S. Gao, *Inorg. Chem.* **2007**, *46*, 2541-2555.
- [21] T. J. Mooibroek, P. Gamez, *CrystEngComm* **2013**, *15*, 1802-1805.
- [22] T. M. Pfaffeneder, S. Thallmair, W. Bauer, B. Weber, *New J. Chem.* **2011**, *35*, 691-700.
- [23] a) L. Zhang, G.-C. Xu, H.-B. Xu, V. Mereacre, Z.-M. Wang, A. K. Powell, S. Gao, *Dalton Trans.* **2010**, *39*, 4856-4868; b) L. Zhang, G.-C. Xu, Z.-M. Wang, S. Gao, *Eur. J. Inorg. Chem.* **2013**, *2013*, 1043-1048.
- [24] a) W. Phonsri, V. Martinez, C. G. Davies, G. N. L. Jameson, B. Moubaraki, K. S. Murray, *Chem. Commun.* **2016**, *52*, 1443-1446; b) S. Hayami, K. Hiki, T. Kawahara, Y. Maeda, D. Urakami, K. Inoue, M. Ohama, S. Kawata, O. Sato, *Chem. Eur. J.* **2009**, *15*, 3497-3508.
- [25] A. Hauser, in *Spin Crossover in Transition Metal Compounds I*, Vol. 233 (Eds.: P. Gütllich, H. A. Goodwin), Springer Berlin Heidelberg, **2004**, pp. 49-58.
- [26] a) M. Griffin, S. Shakespeare, H. J. Shepherd, C. J. Harding, J.-F. Letard, C. Desplanches, A. E. Goeta, J. A. K. Howard, A. K. Powell, V. Mereacre, Y. Garcia, A. D. Naik, H. Müller-Bunz, G. G. Morgan, *Angew. Chem. Int. Ed.* **2011**, *50*, 896-900; b) K. Bhar, S. Khan, J. S. Costa, J. Ribas, O. Roubeau, P. Mitra, B. K. Ghosh, *Angew. Chem. Int. Ed.* **2012**, *51*, 2142-2145; c) H. Watanabe, N. Bréfuel, E. Collet, L. Toupet, K. Tanaka, J.-P. Tuchagues, *Eur. J. Inorg. Chem.* **2013**, *2013*, 710-715; d) S. Bonnet, M. A. Siegler, J. S. Costa, G. Molnar, A. Bousseksou, A. L. Spek, P. Gamez, J. Reedijk, *Chem. Commun.* **2008**, 5619-5621; e) M. Buron-Le Cointe, N. Ould Moussa, E. Trzop, A. Moréac, G. Molnar, L. Toupet, A. Bousseksou, J. F. Letard, G. S. Matouzenko, *Phys. Rev. B* **2010**, *82*, 214106; f) R. G. Miller, S. Narayanaswamy, J. L. Tallon, S. Brooker, *New J. Chem.* **2014**, *38*, 1932-1941; g) K. D. Murnaghan, C. Carbonera, L. Toupet, M. Griffin, M. M. Dîrtu, C. Desplanches, Y. Garcia, E. Collet, J.-F. Letard, G. G. Morgan, *Chem. Eur. J.* **2014**, *20*, 5613-5618; h) B. J. C. Vieira, J. T. Coutinho, I. C. Santos, L. C. J. Pereira, J. C. Waerenborgh, V. da Gama, *Inorg. Chem.* **2013**, *52*, 3845-3850; i) N. Ortega-Villar, M. Muñoz, J. Real, *Magnetochemistry* **2016**, *2*, 16.
- [27] M. A. Halcrow, in *Spin-Crossover Materials* (Ed.: M. A. Halcrow), John Wiley & Sons Ltd, **2013**, 147-169.
- [28] C. M. Klug, A. M. McDaniel, S. R. Fiedler, K. A. Schulte, B. S. Newell, M. P. Shores, *Dalton Trans.* **2012**, *41*, 12577-12585.
- [29] a) J.-F. Létard, G. Chastanet, P. Guionneau, C. Desplanches, in *Spin-Crossover Materials*, John Wiley & Sons Ltd, **2013**, 475-506; b) J.-F. Létard, L. Capes, G. Chastanet, N. Moliner, S. Létard, J.-A. Real, O. Kahn, *Chem. Phys. Lett.* **1999**, *313*, 115-120.
- [30] J.-F. Letard, *J. Mater. Chem.* **2006**, *16*, 2550-2559.
- [31] A. Hauser, *Coord. Chem. Rev.* **1991**, *111*, 275-290.
- [32] O. Hietsoi, P. W. Dunk, H. D. Stout, A. Arroyave, K. Kovnir, R. E. Irons, N. Kassenova, R. Erkasov, C. Achim, M. Shatruck, *Inorg. Chem.* **2014**, *53*, 13070-13077.
- [33] a) F. Neese, *Coord. Chem. Rev.* **2009**, *253*, 526-563; b) M. Schmidt, D. Wiedemann, B. Moubaraki, N. F. Chilton, K. S. Murray, K. R. Vignesh, G. Rajaraman, A. Grohmann, *Eur. J. Inorg. Chem.* **2013**, *2013*, 958-967.
- [34] S. Ye, F. Neese, *Inorg. Chem.* **2010**, *49*, 772-774.
- [35] M. Swart, *J. Chem. Theory Comput.* **2008**, *4*, 2057-2066.
- [36] M. Paez-Espejo, M. Sy, K. Boukheddaden, *J. Am. Chem. Soc.* **2016**, *138*, 3202-3210.
- [37] B. Le Guennic, S. Borshch, V. Robert, *Inorg. Chem.* **2007**, *46*, 11106-11111.
- [38] G.M. Sheldrick, *SADABS, Program for Area Detector Adsorption Correction*, Institute for Inorganic Chemistry, University of Göttingen, Germany, **1996**.
- [39] T. M. McPhillips, S. E. McPhillips, H.-J. Chiu, A. E. Cohen, A. M. Deacon, P. J. Ellis, E. Garman, A. Gonzalez, N. K. Sauter, R. P. Phizackerley, S. M. Soltis, P. Kuhn, *J. Synchrotron Radiat.* **2002**, *9*, 401-406.
- [40] W. Kabsch, *J. Appl. Crystallogr.* **1993**, *26*, 795-800.
- [41] F. Jensen, *Introduction to Computational Chemistry, 2nd Edition*, 2 ed., John Wiley & Sons Ltd, **2007**.
- [42] M. J. Frisch, G. W. Trucks, H. B. Schlegel, G. E. Scuseria, M. A. Robb, J. R. Cheeseman, G. Scalmani, V. Barone, B. Mennucci, G. A. Petersson, H. Nakatsuji, M. Caricato, X. Li, H. P. Hratchian, A. F. Izmaylov, J. Bloino, G. Zheng, J. L. Sonnenberg, M. Hada, M. Ehara, K. Toyota, R. Fukuda, J. Hasegawa, M. Ishida, T. Nakajima, Y. Honda, O. Kitao, H. Nakai, T. Vreven, J. A. Montgomery Jr., J. E. Peralta, F. Ogliaro, M. J. Millam, M. Klene, J. E. Knox, J. B. Cross, V. Bakken, C. Adamo, J. Jaramillo, R. Gomperts, R. E. Stratmann, O. Yazyev, A. J. Austin, R. Cammi, C. Pomelli, J. W. Ochterski, R. L. Martin, K. Morokuma, V. G. Zakrzewski, G. A. Voth, P. Salvador, J. J. Dannenberg, S. Dapprich, A. D. Daniels, Ö. Farkas, J. B. Foresman, J. V. Ortiz, J. Cioslowski, D. J. Fox, Gaussian, Inc., Wallingford, CT, USA, **2009**.
- [43] A. D. Becke, *J. Chem. Phys.* **1993**, *98*, 5648-5652.
- [44] a) C. Lee, W. Yang, R. G. Parr, *Phys. Rev. B* **1988**, *37*, 785-789; b) B. Miehlich, A. Savin, H. Stoll, H. Preuss, *Chem. Phys. Lett.* **1989**, *157*, 200-206.
- [45] a) A. Schäfer, H. Horn, R. Ahlrichs, *J. Chem. Phys.* **1992**, *97*, 2571-2577; b) A. Schäfer, C. Huber, R. Ahlrichs, *J. Chem. Phys.* **1994**, *100*, 5829-5835.
- [46] D. C. Ashley, E. Jakubikova, *Coord. Chem. Rev.* **2017**, *337*, 97-111.
- [47] J. Nance, D. N. Bowman, S. Mukherjee, C. T. Kelley, E. Jakubikova, *Inorg. Chem.* **2015**, *54*, 11259-11268.
- [48] D. N. Bowman, E. Jakubikova, *Inorg. Chem.* **2012**, *51*, 6011-6019.
- [49] J. Sirirak, W. Phonsri, D. J. Harding, P. Harding, P. Phommon, W. Chaoprasa, R. M. Hendry, T. M. Roseveare, H. Adams, *J. Mol. Struct.* **2013**, *1036*, 439-446.

## Entry for the Table of Contents (Please choose one layout)

Layout 1:

## FULL PAPER

A family of Fe(II) spin crossover complexes containing N<sub>2</sub>O Schiff base ligands, [Fe<sup>II</sup>(qsal-X)<sub>2</sub>] where X = F (1), Cl (2), Br (3), I (4), has been investigated in detail. Most of the compounds show abrupt spin transitions, at or above room temperature. Important knowledge for the design of new spin crossover materials is discussed



Wasinee Phonsri, David S. Macedo, Kuduva R. Vignesh, Gopalan Rajaraman, Casey G. Davies, Guy N. L. Jameson, Boujemaa Moubarak, Jas S. Ward, Paul E. Kruger, Guillaume Chastanet, and Keith S. Murray\*

Page No. – Page No.

**Halogen substitution effects on N<sub>2</sub>O Schiff base ligands in unprecedented abrupt Fe(II) spin crossover complexes including one showing symmetry breaking**

- [a] Dr W. Phonsri, D. S. Macedo, Dr B. Moubarek, School of Chemistry, Building 23, Monash University, Clayton, Victoria, 3800, Australia. E-mail: keith.murray@monash.edu
- [b] K. R. Vignesh, IITB-Monash Research Academy, IIT Bombay, Mumbai, 400076, India
- [c] Prof G. Rajaraman, Department of Chemistry, Indian Institute of Technology Bombay, Mumbai, 400076, India
- [d] C. G. Davies, Dr. G. N. L. Jameson, Department of Chemistry & MacDiarmid Institute for Materials and Nanotechnology, University of Otago, Dunedin, 9054, New Zealand
- [e] Dr J. S. Ward, Prof P. E. Kruger, Department of Chemistry & MacDiarmid Institute for Materials and Nanotechnology, University of Canterbury, Private Bag 4800, Christchurch 8041, New Zealand
- [f] Dr G. Chastanet, CNRS, Université de Bordeaux, ICMCB, 8 Avenue Schweitzer, Pessac 33608, France

Supporting information for this article is given in the supplementary material. (Please delete this text if not appropriate)

## SUPPORTING INFORMATION

### **Halogen substitution effects on N<sub>2</sub>O Schiff base ligands in unprecedented abrupt Fe(II) spin crossover complexes including one showing symmetry breaking**

Wasinee Phonsri,<sup>[a]</sup> David S. Macedo,<sup>[a]</sup> Kuduva R. Vignesh,<sup>[b]</sup> GopalanRajaraman,<sup>[c]</sup> Casey G. Davies,<sup>[d]</sup> Guy N. L. Jameson,<sup>[d]</sup> Boujemaa Moubaraki,<sup>[a]</sup> Jas S. Ward,<sup>[e]</sup> Paul E. Kruger,<sup>[e]</sup> Guillaume Chastanet,<sup>[f]</sup> and Keith S. Murray<sup>\*[a]</sup>

[a] School of Chemistry, Monash University, Clayton, Victoria, 3800, Australia

[b] IITB-Monash Research Academy, IIT Bombay, Mumbai, 400076, India

[c] Department of Chemistry, Indian Institute of Technology, Mumbai, 400076, India

[d] Department of Chemistry & MacDiarmid Institute for Advanced Materials and Nanotechnology, University of Otago, Dunedin, 9054, New Zealand

[e] Department of Chemistry&MacDiarmid Institute for Advanced Materials and Nanotechnology, University of Canterbury,Private Bag 4800, Christchurch 8041, New Zealand.

[f] CNRS, Université de Bordeaux, ICMCB, 87 avenue du Dr. A. Schweitzer, Pessac 33608, France

## Table of Contents

**Table S1** Crystallographic data, CCDC numbers and structure refinement for iron(III) complexes

**Table S2** Selected bond lengths and octahedral distortion parameters for iron(III) complexes

**Table S3** Intermolecular interactions in **1** at 123 K

**Table S4** Intermolecular interactions in  $[\text{Fe}(\text{qsal-X})_2]$  where X = Cl **2** and Br **3**

**Table S5** Intermolecular interaction in  $[\text{Fe}(\text{qsal-X})_2]$  where X = Cl **2** and Br **3** (continued)

**Table S6** Intermolecular interactions in  $[\text{Fe}(\text{qsal-I})_2] \cdot \text{CH}_2\text{Cl}_2$  at 100 K and  $[\text{Fe}(\text{qsal-I})_2] \cdot 0.3\text{CH}_2\text{Cl}_2$  at 298 K

**Table S7** Intermolecular interactions in  $[\text{Fe}(\text{qsal-I})_2]\text{Cl}$  at 100 K

**Table S8** Fe-L bond lengths for the present and reported Fe(II) complexes with  $\text{N}_2\text{O}$  tridentate ligands

**Table S9** Calculated  $\Delta H$  and  $\Delta S$  values from DSC results of the compounds **2**, **3**, **4**

**Table S10** B3LYP optimized selected bond parameters for complex **2** - **4** and **4'** (See Figure S1 for atoms labelling).

**Figure S1** The asymmetric unit components for the iron(II) and iron(III) compounds with atom labels

**Figure S2** Representations of compound **1** at 123 K for a) C-H $\cdots$ O/F interactions b)  $\pi$ - $\pi$  interactions c) and d) *pseudo*-3D packing

**Figure S3** *Pseudo* 3D packing of **2** at 100 K representing the halogen atoms occupying positions along the *c* axis of the unit cell

**Figure S4** The packing of intermediate phases of a) **2** at 308 K and b)  $[\text{Fe}(\text{qsal-Br})_2]\text{NO}_3 \cdot 2\text{MeOH}^{[1]}$  at 175 K (blue is LS, orange is HS)

**Figure S5** A packing in a layer via C-Br $\cdots$ H and C-I $\cdots$  $\pi$  interactions in a) **3** and b) **4** at 100 K

**Figure S6** Representation of the main interactions in **4'** packing at 100 K

**Figure S7** Plot of variable-temperature magnetic susceptibilities ( $\chi_M T$ ) for compound **1**

**Figure S8** a) Cyclic voltammograms of 0.3 mM **2**, **3** and Hqsal-Br ligand with 0.1 M  $[\text{Bu}_4\text{N}]^+[\text{PF}_6]^-$  electrolyte in DMF. The oxidation at around 400 mV is attributed to the Hqsal-X ligand, while the reduction at *ca.* -500 mV is due to the  $\text{Fe}^{3+}/\text{Fe}^{2+}$  redox couple. Steady-state voltammograms obtained at a 33  $\mu\text{m}$  diameter carbon micro electrode in 0.3 mM of b) **2** and c) **3** in DMF with a scan rate of 0.01  $\text{V s}^{-1}$  confirming the Fe(III) species present in the solution. d) X-band EPR spectra of **2** (green), **3** (red) and  $[\text{Fe}(\text{III})\text{qsal-Cl}]\text{CF}_3\text{SO}_3^{[9]}$  (blue) at RT.

**Figure S9** Thermal behaviour of the  $\chi_M T$  product of **3** before irradiation (■), during irradiation (Δ) and in the dark after irradiation (■). Note Photomagnetic measurement on a surface sample. Irradiation at 640 nm for 6 hours, three repeat measurements were made to try to improve the photoconversion efficiency without success. T(LIESST) = 30 K

**Figure S10**  $^{57}\text{Fe}$  Mössbauer spectral plots for **2**, **3** and **4**. Velocity calibrations relative to  $\alpha$ -iron.

**Figure S11** DSC plots for compound a) **2**, b) **3** and c) **4**

**Figure S12** Eigenvalue plots computed for complexes a) **2** and b) **4**.

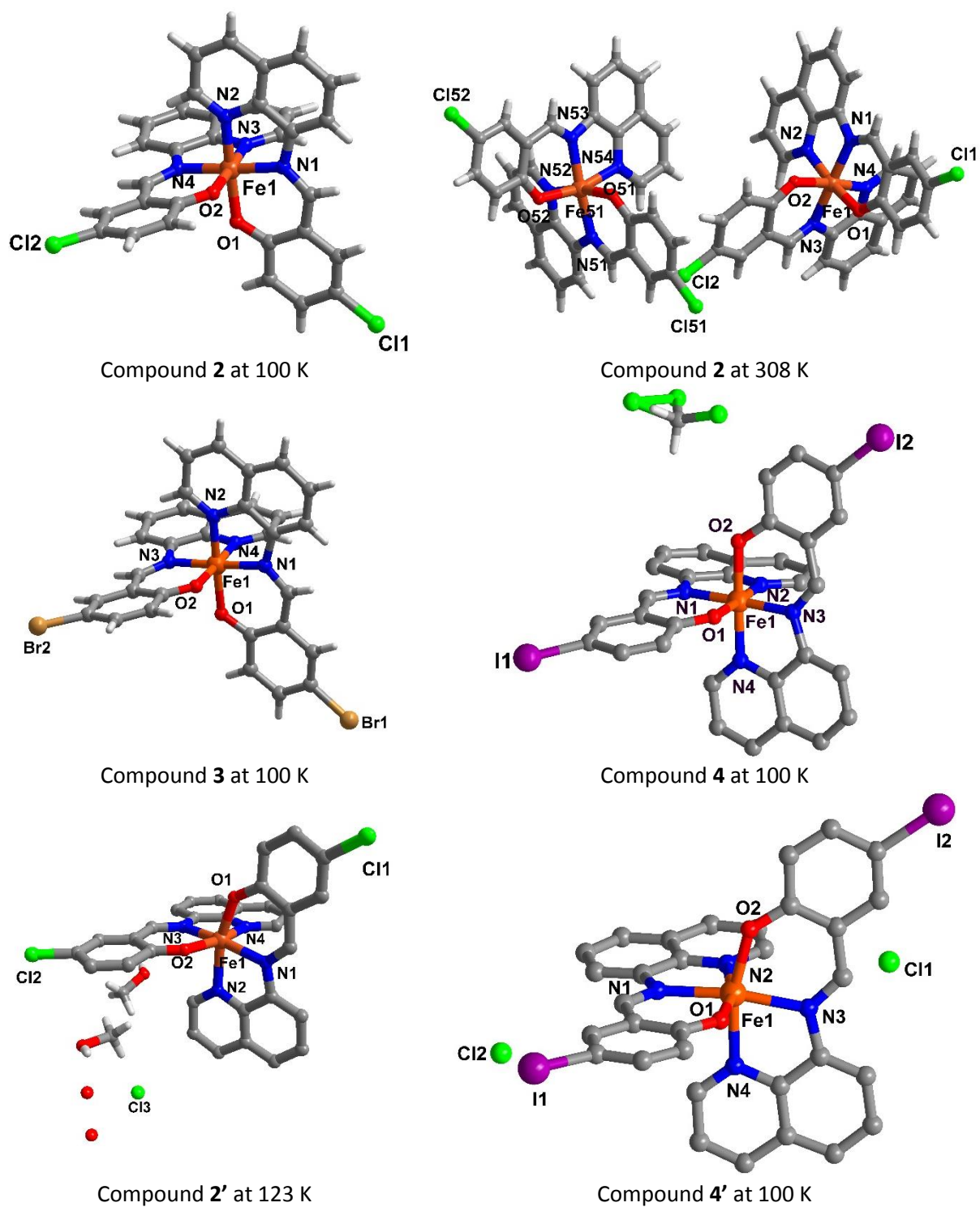
**Figure S13** B3LYP computed spin density plot of the HS state for complex **4'**.

**Table S1** Crystallographic data, CCDC numbers and structure refinement for iron(III) complexes

	<b>2'</b>	<b>Squeeze 2'</b>	<b>4'</b>
	<b>123 K</b>	<b>123 K</b>	<b>100 K</b>
Formula	C <sub>33.50</sub> H <sub>26</sub> Cl <sub>3</sub> FeN <sub>4</sub> O <sub>5</sub>	C <sub>32</sub> H <sub>20</sub> Cl <sub>3</sub> FeN <sub>4</sub> O <sub>2</sub>	C <sub>32</sub> H <sub>20</sub> ClFe <sub>2</sub> N <sub>4</sub> O <sub>2</sub>
Molecular weight / gmol <sup>-1</sup>	726.78	654.72	837.62
Crystal system	Triclinic	Triclinic	Triclinic
Space group	P $\bar{1}$	P $\bar{1}$	P $\bar{1}$
<i>a</i> / Å	11.0351 (3)	11.0351 (3)	10.703 (2)
<i>b</i> / Å	12.6565 (4)	12.6565 (4)	12.639 (3)
<i>c</i> / Å	13.4613 (4)	13.4613 (4)	13.962 (3)
$\alpha$ / °	62.789 (1)	62.789 (1)	63.91 (3)
$\beta$ / °	72.313 (1)	72.313 (1)	74.90 (3)
$\gamma$ / °	72.202 (1)	72.202 (1)	74.88 (3)
Cell volume / Å <sup>3</sup>	1561.83 (8)	1561.83 (8)	1614.3 (6)
Z	2	2	2
Absorption coefficient / mm <sup>-1</sup>	0.790	0.774	2.497
Reflections collected	35890	35932	62171
Independent reflections, <i>R</i> <sub>int</sub>	8834, 0.0357	8838, 0.0357	9301, 0.0772
Max. and min. transmission	0.8907 and 0.8453	0.8907 and 0.8454	0.9755 and 0.9518
Restraints/parameters	1/427	0/379	0/383
Goodness of fit	1.043	1.031	1.083
Final R indices [ <i>I</i> > 2σ( <i>I</i> ): <i>R</i> <sub>1</sub> , <i>wR</i> <sub>2</sub>	0.0650, 0.2016	0.0491, 0.1471	0.0663, 0.2044
CCDC No.	1495814	1495814	1495818

**Table S2** Selected bond lengths and octahedral distortion parameters for iron(III) complexes

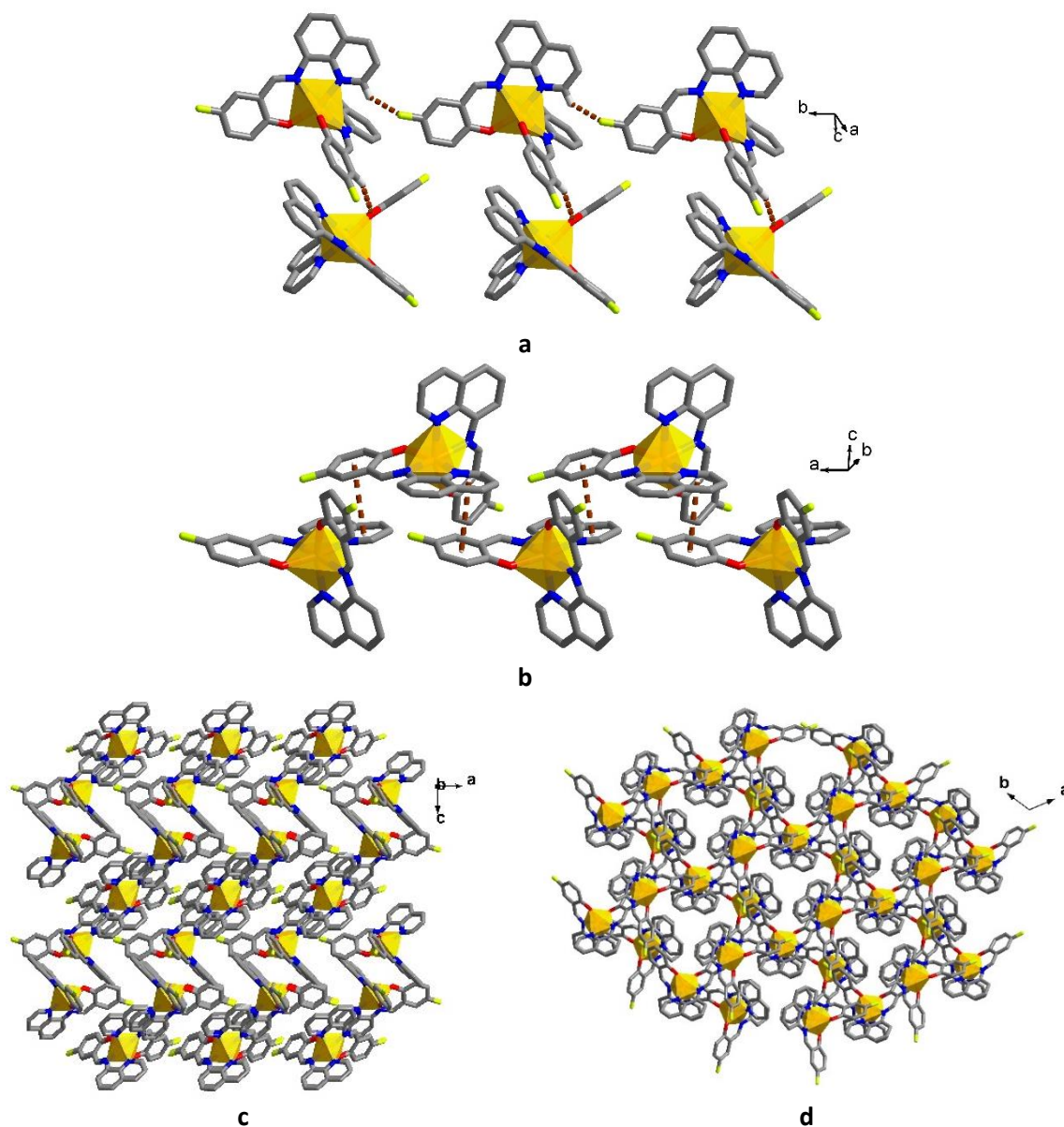
	<b>[Fe(qsal-Cl)<sub>2</sub>]Cl·1.5H<sub>2</sub>O·1.5MeOH, 2'</b>	<b>[Fe(qsal-I)<sub>2</sub>]Cl, 4'</b>
	<b>123 K</b>	<b>100 K</b>
Fe1-O1/Å	1.909 (2)	1.928 (4)
Fe1-O2/Å	1.920 (2)	1.930 (4)
Fe1-N1/Å	2.124 (3)	2.125 (4)
Fe1-N2 /Å	2.156 (3)	2.152 (4)
Fe1-N3/Å	2.127 (3)	2.124 (4)
Fe1-N4 /Å	2.149 (3)	2.145 (4)
Σ/°	71	68
Θ/°	218	200



**Figure S1** The asymmetric unit components for the iron(II) and iron(III) compounds with atom labels

**Table S3** Intermolecular interactions in **1** at 123 K

Interactions	Distance/Å
A chain along <i>a</i> axis	
$\pi$ - $\pi$	3.597
A chain along <i>c</i> axis	
C5-F5...O1	2.4138(14)
C14-H14...O1	2.7061(15)
A chain along <i>b</i> axis	
C15-H15...F1	2.2898(17)

**Figure S2** Representations of compound **1** at 123 K for a) C-H...O/F interactions b)  $\pi$ - $\pi$  interactions c) and d) *pseudo*-3D packing

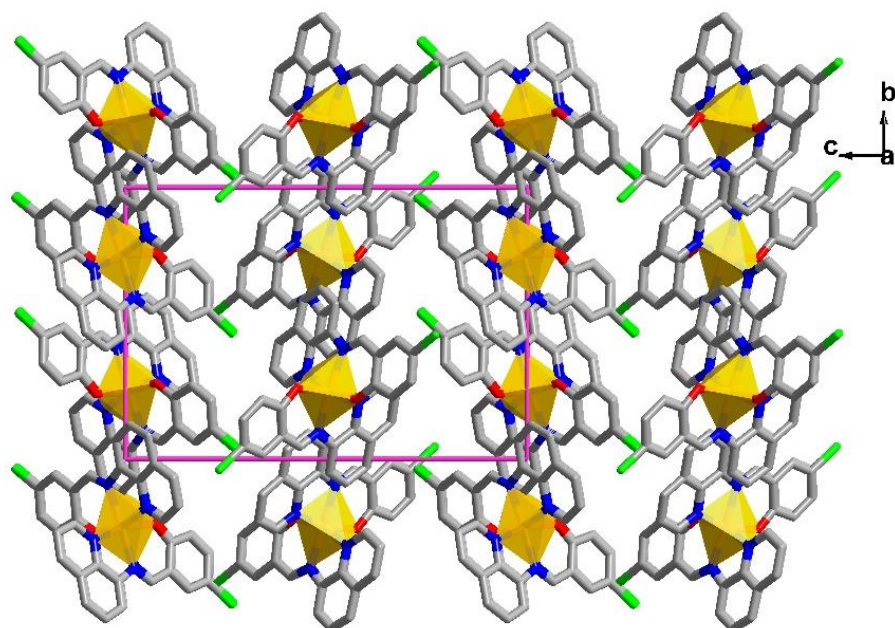


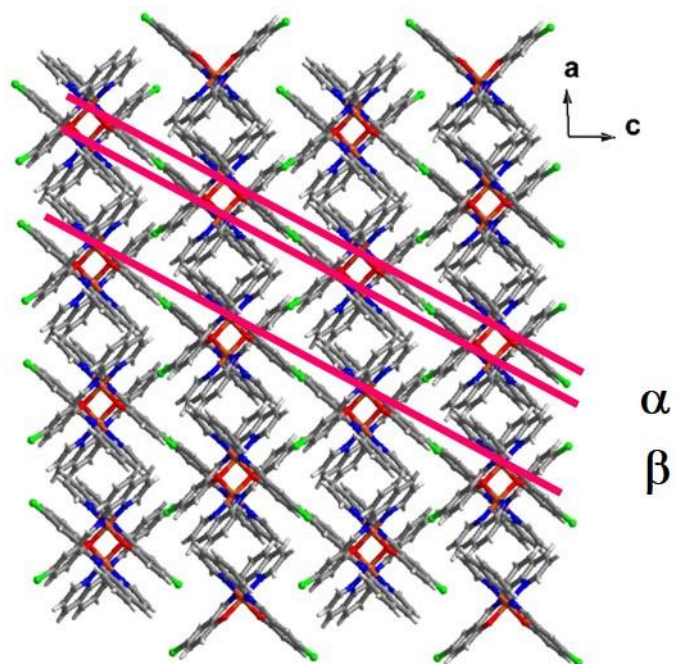
**Figure S3** *Pseudo* 3D packing of **2** at 100 K representing the halogen atoms occupying positions along the *c* axis of the unit cell

**Table S4** Intermolecular interactions in [Fe(qsal-X)<sub>2</sub>] where X = Cl **2** and Br **3**

	[Fe(qsal-Cl) <sub>2</sub> ], <b>2</b>						[Fe(qsal-Br) <sub>2</sub> ], <b>3</b>	
	100 K	298 K	308 K	312 K	318 K	330 K	100 K	380 K
A chain along <i>b</i> axis								
$\pi$ - $\pi$	3.304	3.352	3.386	3.406	3.427	3.436	3.254	3.368
$\pi$ - $\pi$	3.213	3.258	3.282	3.307	3.312	3.330	3.234	3.376
C9-H9...O2	2.4323(0)	2.4739(0)	2.4784(1)	2.4460(1)	2.4653(0)	2.4701(1)	2.4436(29)	2.4931(1)
C23-H23...O1	2.6129(0)	2.6624(0)	2.6750(1)	2.6718(1)	2.7078(1)	2.7174(1)	2.5948(27)	2.7335(1)
C21-H21...O1	2.8901(0)	2.9855(0)	2.9405(1)	2.8553(1)	2.7773(1)	2.7437(1)	2.8454(27)	2.6439(1)
$\pi$ - $\pi$			3.414	3.416				
$\pi$ - $\pi$			3.292	3.301				
C59-H59...O52			2.4600(1)	2.3392(1)				
C73-H73...O51			2.7077(1)	2.6771(1)				
A chain along <i>c</i> axis								
C2-H2...X1								
Van Der Waals Radius H = 1.2, Cl = 1.75, Br = 1.85 Å	2.9594(0)	3.041(0)	3.0476(1)(Cl1-H52)	3.0553(1)(Cl1-H52)	2.9972(1)	2.9944(1)	2.9763(7)	3.0625(1)
$\pi$ - $\pi$	3.296	3.360	3.450(C19-C80)	3.478(C19-C80)	3.489	3.512	3.405	3.618
$\pi$ - $\pi$	3.349	3.431	3.559(C3-C64)	3.568(C3-C64)	3.560	3.587	3.511	3.812
A chain along <i>a</i> axis								
P4AE1								
$\pi$ - $\pi$	3.555	3.598	3.610	3.562	3.486	3.471	3.598	3.523
C26-H26... $\pi$	2.850	2.964	2.830	3.001	3.016	3.084	2.862	3.144
P4AE2								
$\pi$ - $\pi$	3.556	3.594	3.625	3.615	3.596	3.597	3.618	3.638
C11-H11... $\pi$	2.664	2.727	2.580	2.754	2.749	2.844	3.374	3.430
P4AE51								
$\pi$ - $\pi$			3.470	3.475				
C76-H76... $\pi$			3.005	3.121				
P4AE52								
$\pi$ - $\pi$			3.569	3.578				
C61-H61... $\pi$			2.680	2.741				
C18-H18...X2	2.8334(0)	2.9045(0)	2.9177(1)(Cl2-H68) 2.7889(1)(Cl52-H18)	2.8865(1)(Cl2-H68) 2.7763(1)(Cl52-H18)	2.8113(1)	2.8021(1))	2.8442(7)	2.8236(1)

**Table S5** Intermolecular interaction in  $[\text{Fe}(\text{qsal-X})_2]$  where X = Cl **2** and Br **3** (continued)

	$[\text{Fe}(\text{qsal-Cl})_2]$ , <b>2</b>						$[\text{Fe}(\text{qsal-Br})_2]$ , <b>3</b>	
	100 K	298 K	308 K	312 K	318 K	330 K	100 K	380 K
$\alpha$ planar Fe1-Fe1 plane to plane between 2 $\pi$ - $\pi$ in a chain, along <i>b</i> axis Fe1, Fe51	2.288	2.252	2.248, 2.041	2.204, 2.058	2.103	2.079	2.310	2.159
$\beta$ planar Fe1-Fe1 plane to plane between 2 P4AE, along <i>b</i> axis Fe1, Fe51	6.970	7.016	7.107, 7.314	7.177, 7.322	7.308	7.361	7.009	7.421



The planar distance of the Fe(II) in the same  $\pi$ - $\pi$  chain,  $\alpha$ , reduces from LS towards HS, but  $\beta$  (inter-planar distance between Fe(II) interacting via P4AE) increase.

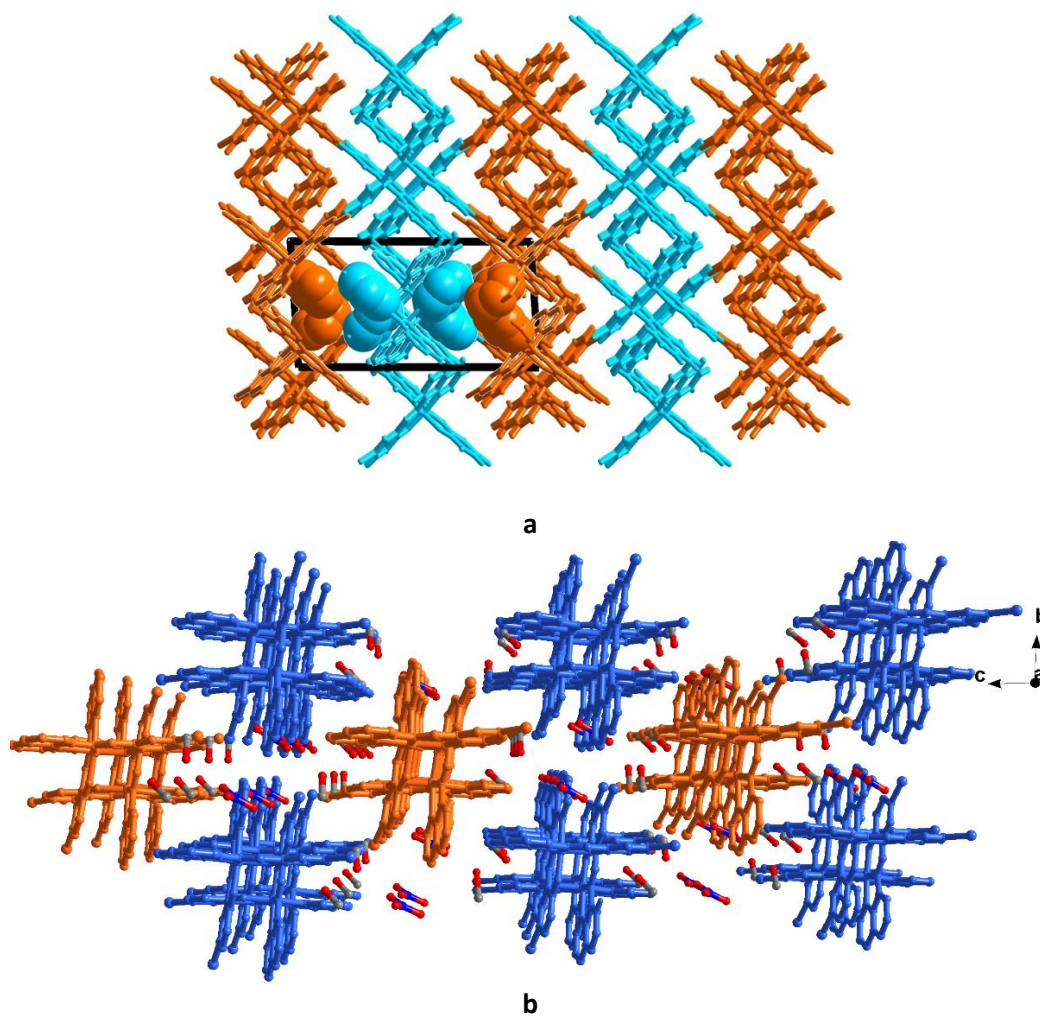


**Figure S4** The packing of intermediate phases of a) **2** at 308 K and b)  $[\text{Fe}(\text{qsal-Br})_2]\text{NO}_3 \cdot 2\text{MeOH}^{[1]}$  at 175 K (blue is LS, orange is HS)

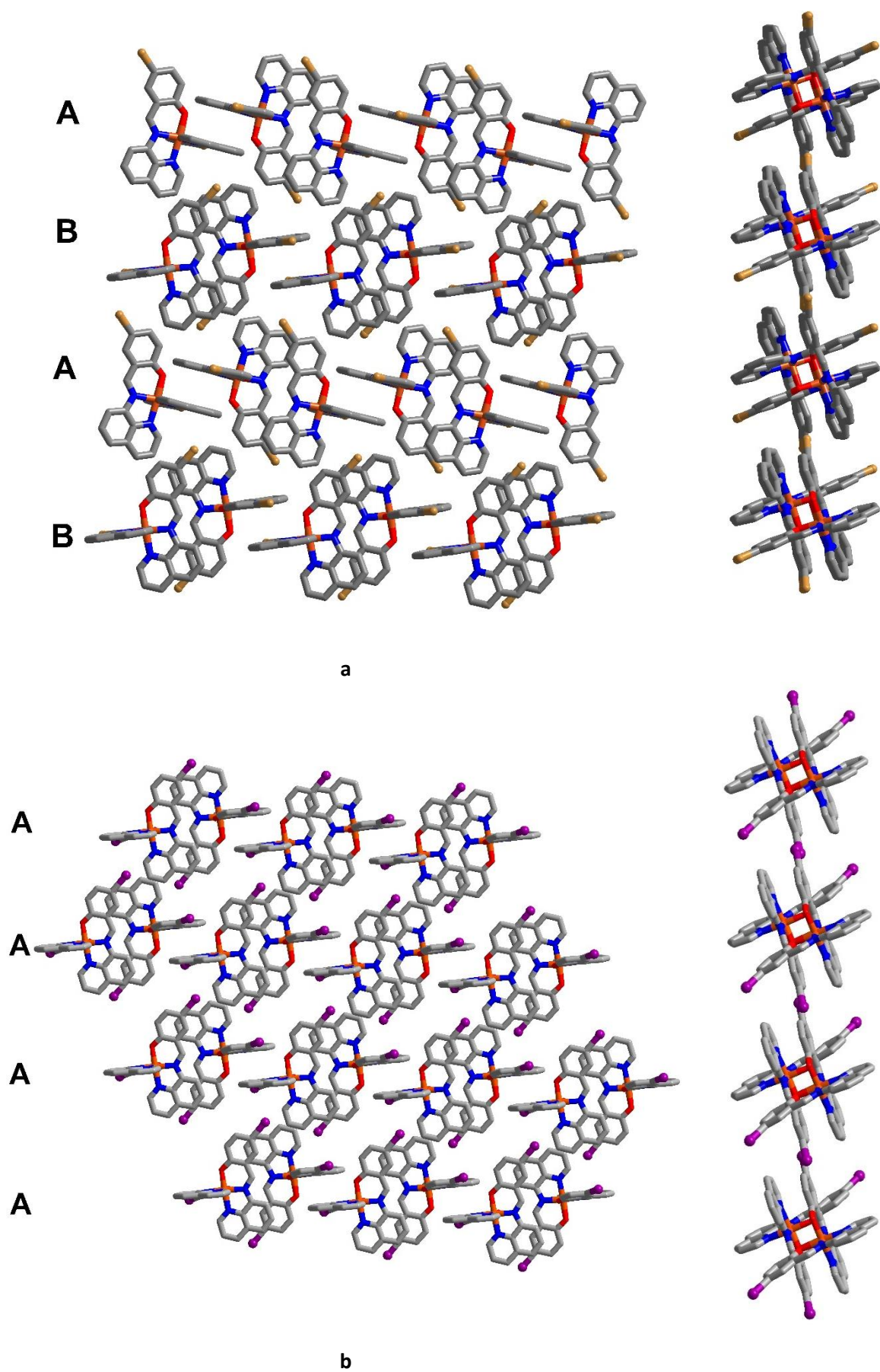


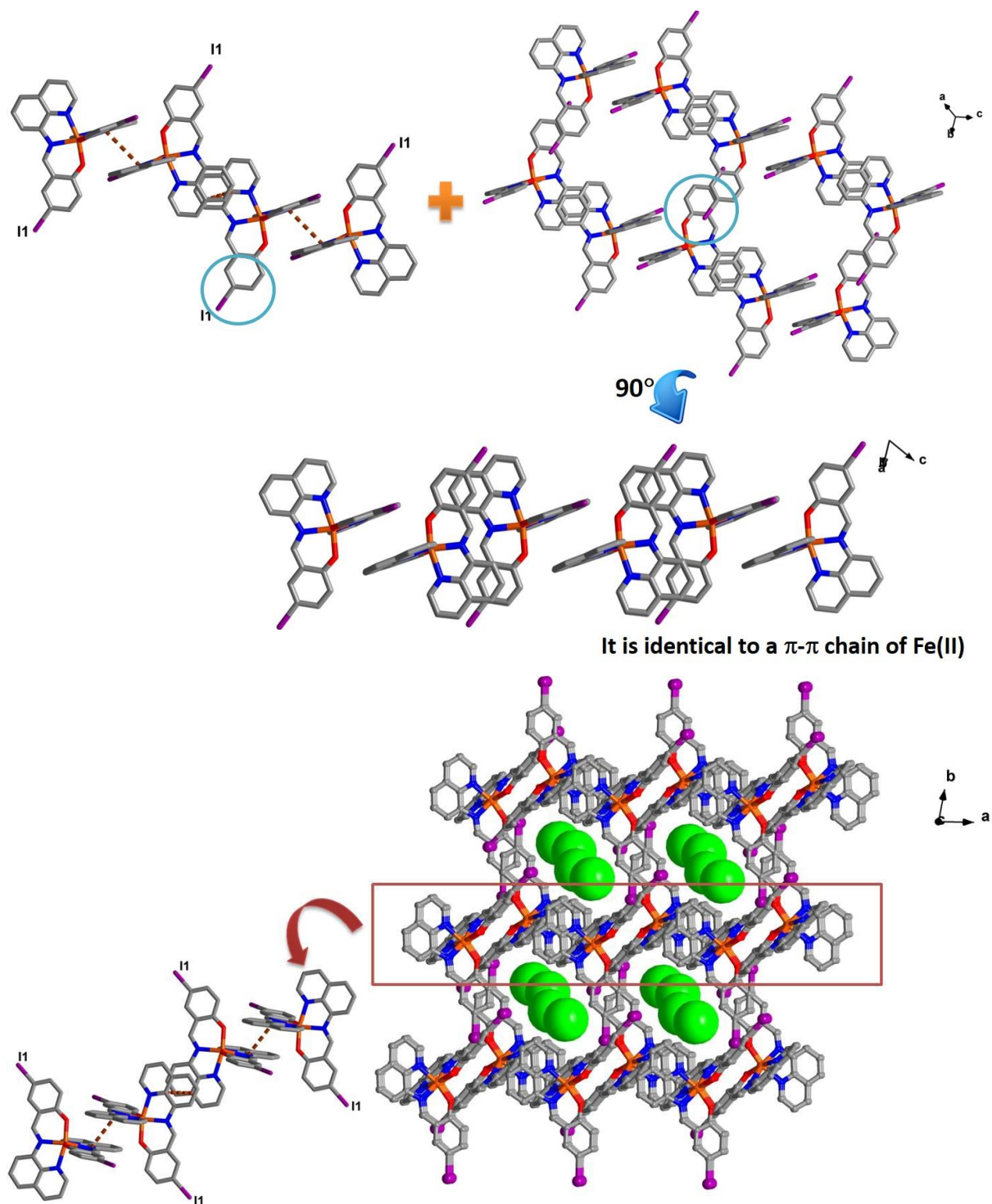
**Figure S5** A packing in a layer *via* C-Br...H and C-I... $\pi$  interactions in a) **3** and b) **4** at 100 K

**Table S6** Intermolecular interactions in  $[\text{Fe}(\text{qsal-I})_2]\cdot\text{CH}_2\text{Cl}_2$  at 100 K and  $[\text{Fe}(\text{qsal-I})_2]\cdot 0.3\text{CH}_2\text{Cl}_2$  at 298 K

Interactions/Å	100 K	298 K
A chain along <i>c</i> axis		
$\pi$ - $\pi$	3.249	3.304
$\pi$ - $\pi$	3.227	3.314
C7-H7...O2	2.6305(41)	2.8197(70)
C9-H9...O2	2.6197(32)	2.7571(62)
C23-H23...O1	2.7020(36)	2.7802(65)
C25-H25...O1	2.5412(31)	2.5670(59)
A chain along <i>a</i> axis		
C20-I2... $\pi$	3.675	3.983
A chain along <i>b</i> axis		
P4AE		
$\pi$ - $\pi$	2.958	2.777
C13-H13... $\pi$	3.258	3.271
C15-H15...I1	3.0354(10)	3.2160(14)
C4-I1... $\pi$	3.581	3.774

**Table S7** Intermolecular interactions in  $[\text{Fe}(\text{qsal-I})_2]\text{Cl}$  at 100 K

A chain along <i>a</i> axis	Distance/Å 100 K
$\pi$ - $\pi$	3.397
$\pi$ - $\pi$	3.372
C25-H25...O1	2.5979(43)
A chain along <i>b</i> axis	
C4-I1...O2	3.2257(37)
$\pi$ - $\pi$	3.566
A chain along <i>c</i> axis	
P4AE	
$\pi$ - $\pi$	3.392
C27-H27... $\pi$	2.806
Cl anion interaction	
C20-I2...Cl1	3.3482(61)
C15-H15...Cl1	2.6826(42)
C5-H5...Cl2	2.7933(62)
C7-H7...Cl2	2.8938(64)
C31-H31...Cl2	2.7354(55)



Author Manuscript

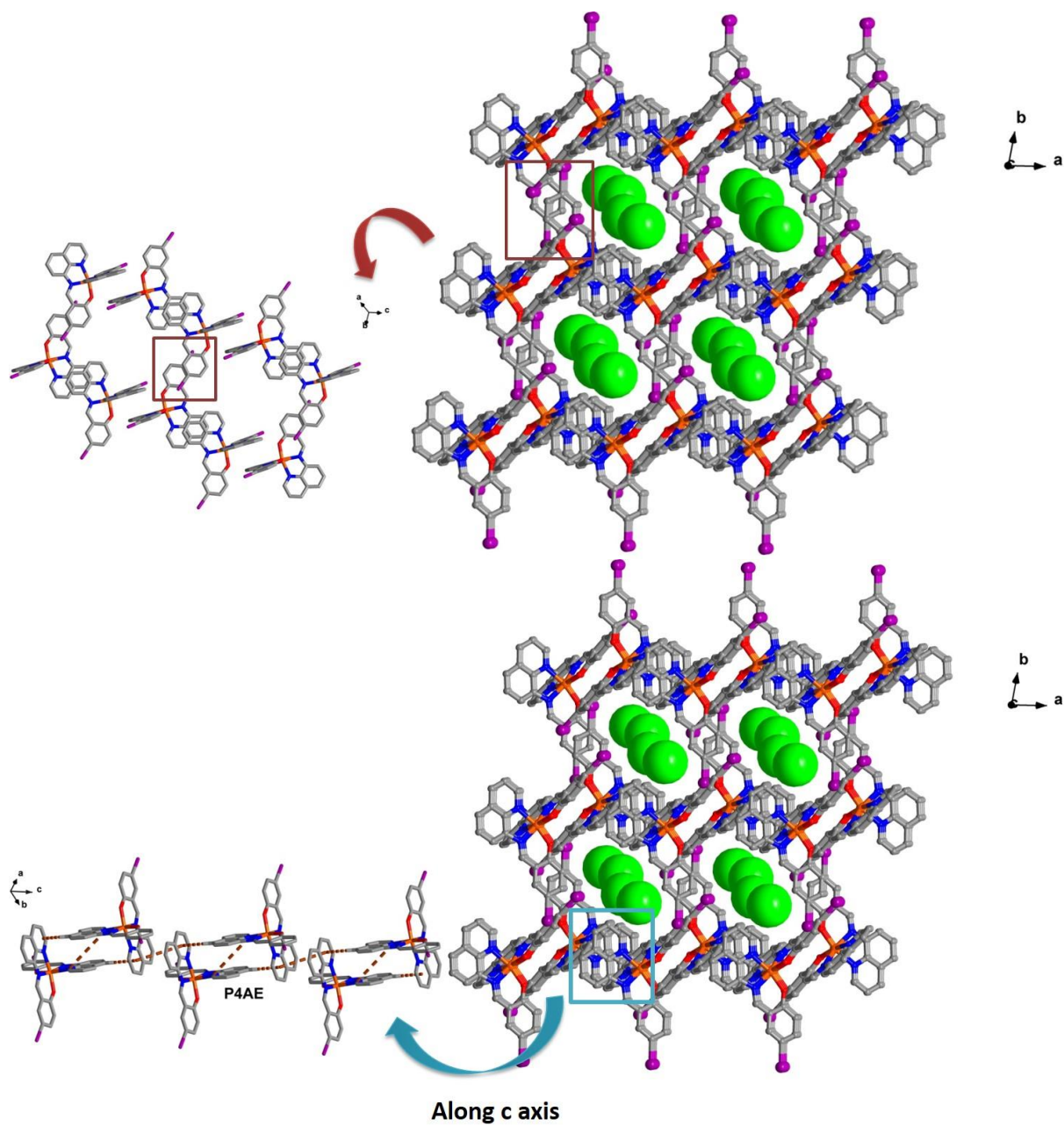


**Figure S6** Representation of the main interactions in 4' packing at 100 K

**Table S8** Fe-L bond lengths for the present and reported Fe(II) complexes with N<sub>2</sub>O tridentate ligands

Complexes	Fe-O <sub>ave</sub> LS	Fe-O <sub>ave</sub> HS	Fe-N <sub>ave</sub> LS	Fe-N <sub>ave</sub> HS	ΔFe-O	ΔFe-N	Ref
Fe(L) <sub>2</sub> ·CH <sub>3</sub> OH	1.983		1.907				[2]
Fe(L) <sub>2</sub>		2.079		2.161			[2]
[Fe(qnal) <sub>2</sub> ].CH <sub>2</sub> Cl <sub>2</sub>	1.942	2.015	1.943	2.164	0.073	0.221	[3]
[Fe(qnal) <sub>2</sub> ]							[3]
[Fe(Hqsalc) <sub>2</sub> ]							[4]
[Fe(qnal-12) <sub>2</sub> ].2C <sub>6</sub> H <sub>6</sub>		2.027		2.174			[4]
Fe(pap-5NO <sub>2</sub> ) <sub>2</sub>							[5]
Fe(qsal-5NO <sub>2</sub> ) <sub>2</sub>							[5]
[Fe(L <sup>2</sup> ) <sub>2</sub> ](OTf) <sub>2</sub>		2.174 <sup>a</sup>		2.138			[6]
Fe(L <sup>1</sup> ) <sub>2</sub>		2.101		2.174			[7]
Fe(L <sup>2</sup> ) <sub>2</sub>	1.996		1.895				[7]
Fe(L <sup>3</sup> ) <sub>2</sub>	1.984		1.966				[7]
Fe(L <sup>4</sup> ) <sub>2</sub>		2.105		2.150			[7]
Fe(L <sup>5</sup> ) <sub>2</sub>	1.995	2.069	1.908	2.053	0.074	0.145	[7]
Fe(L <sup>6</sup> ) <sub>2</sub>	1.979		1.901				[7]
Fe(L1) <sub>2</sub>	1.991	2.082	1.927	2.110	0.091	0.183	[8]
Fe(L2) <sub>2</sub>	1.987		1.912				[8]
[Fe(qsal-F) <sub>2</sub> ] <b>1</b>		2.016		2.178			This work
[Fe(qsal-Cl) <sub>2</sub> ] <b>2</b>	1.958	2.010	1.945	2.154	0.052	0.209	This work
[Fe(qsal-Br) <sub>2</sub> ] <b>3</b>	1.945	2.004	1.950	2.148	0.059	0.198	This work
[Fe(qsal-I) <sub>2</sub> ] <b>4</b>	1.955	2.007	1.943	2.116	0.052	0.173	This work
<b>In average</b>	1.974	2.047	1.927	2.143	0.067	0.141	

An oxygen donor is hydroxyl (Fe-OH), it is therefore longer than normal Fe-O

- [2] L = 4-hydroxy-N'-((pyridin-2-yl)-methylene)-benzohydrazide
- [4] Hqnal-12 = N-(8'-quinolyl)-1-hydroxy-2-naphthalidimine  
H<sub>2</sub>qsalc = 4-hydroxy-3-[(8-quinolinylimino)methyl]benzoic acid
- [6] L<sup>2</sup> = 4-[(6-methanol)-2-pyridyl]-3-aza-3-butenyl)
- [7] HL<sup>1</sup> = N'-((pyridin-2-yl)methylene)benzohydrazide  
HL<sup>2</sup> = N'-(1-(pyridin-2-yl)ethylidene)benzohydrazide  
HL<sup>3</sup> = N'-(phenyl(pyridin-2-yl)methylene)benzohydrazide  
HL<sup>4</sup> = 2-hydroxy-N'-((pyridin-2-yl)methylene)benzohydrazide  
HL<sup>5</sup> = 2-hydroxy-N'-(1-(pyridin-2-yl)ethylidene)benzohydrazide  
HL<sup>6</sup> = 2-hydroxy-N'-(phenyl(pyridin-2-yl)methylene)benzohydrazide
- [8] HL1 = 2-hydroxy-3-methyl-N'-[1-(pyridine-2-yl)-butylidene]benzohydrazide  
HL2 = 2-hydroxy-N'-[1-(pyridine-2-yl)butylidene]benzohydrazide

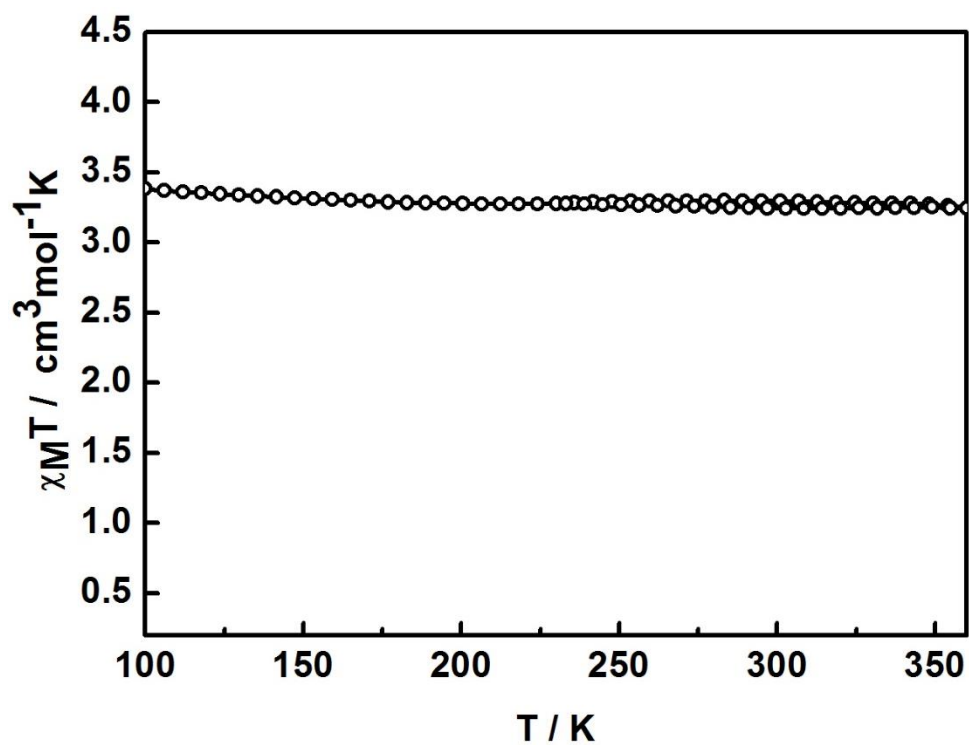
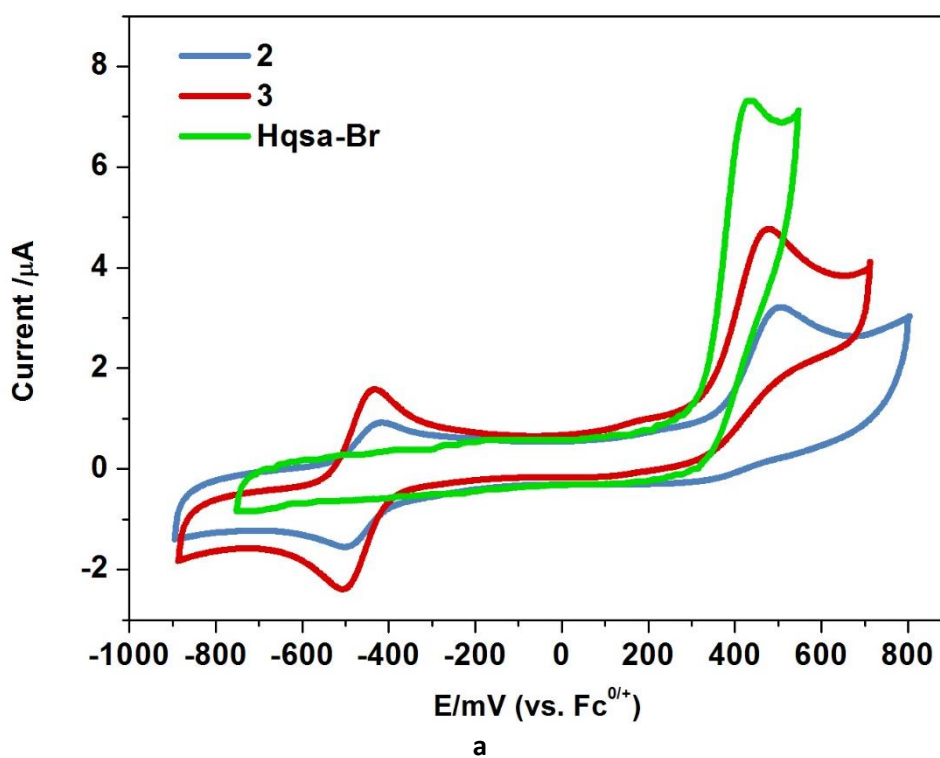
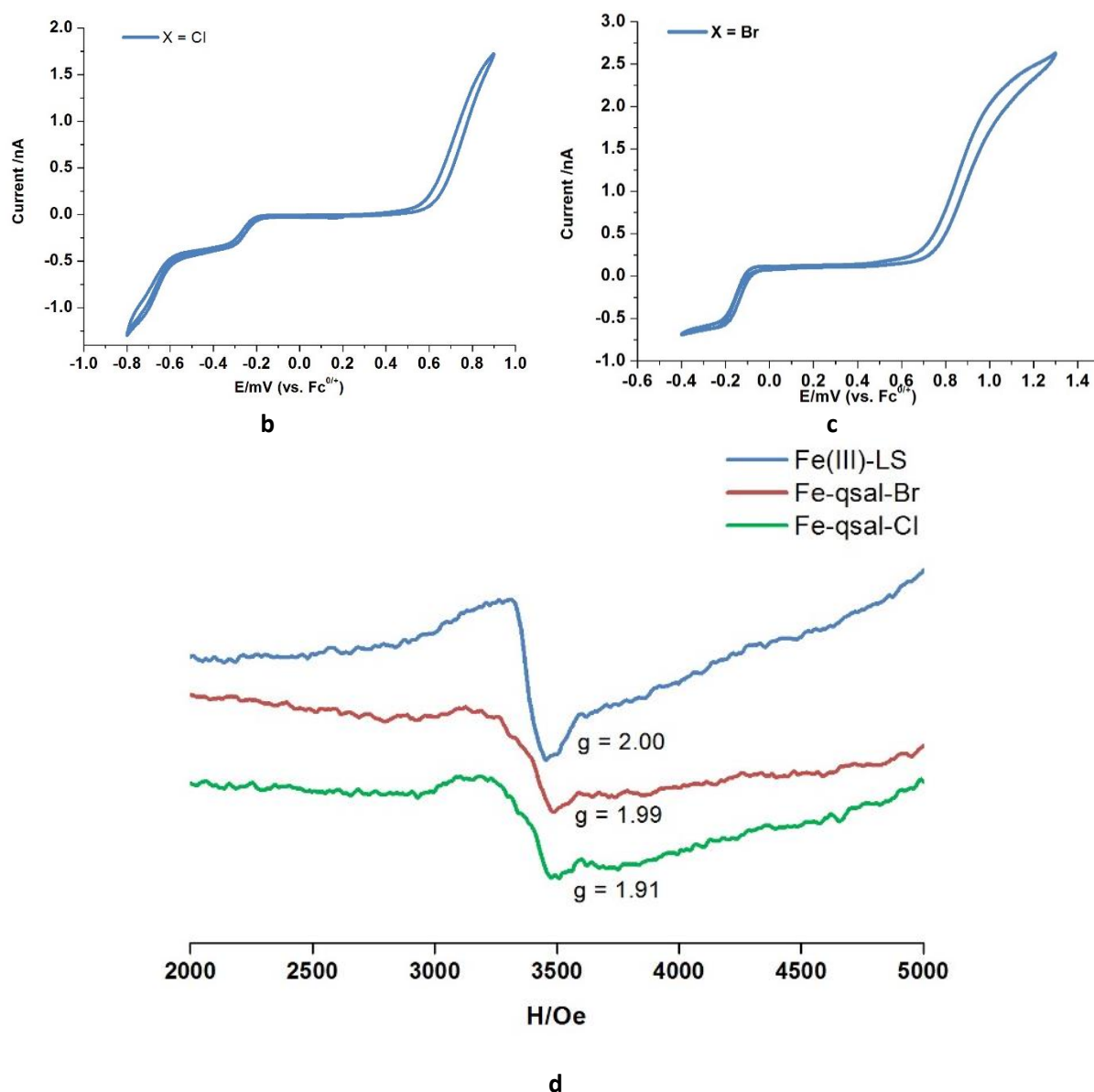


Figure S7 Plot of variable-temperature magnetic susceptibilities ( $\chi_M T$ ) for compound 1





**Figure S8** a) Cyclic voltammograms of 0.3 mM **2**, **3** and Hqsal-Br ligand with 0.1 M  $[\text{Bu}_4\text{N}]^+[\text{PF}_6]^-$  electrolyte in DMF. The oxidation at around 400 mV is attributed to the Hqsal-X ligand, while the reduction at *ca.* -500 mV is due to the  $\text{Fe}^{3+}/\text{Fe}^{2+}$  redox couple. Steady-state voltammograms obtained at a 33  $\mu\text{m}$  diameter carbon micro electrode in 0.3 mM of b) **2** and c) **3** in DMF with a scan rate of  $0.01 \text{ V s}^{-1}$  confirming the Fe(III) species present in the solution. d) X-band EPR spectra of **2** (green), **3** (red) and  $[\text{Fe(III)qsal-Cl}]\text{CF}_3\text{SO}_3$ <sup>[9]</sup> (blue) at RT.

According to cyclic voltammetric data and EPR spectra of **2** and **3** in solution, the results indicate formation of LS Fe(III) at RT. This suggests the instability of **2** and **3** in solution and oxidation, in part, to Fe(III).

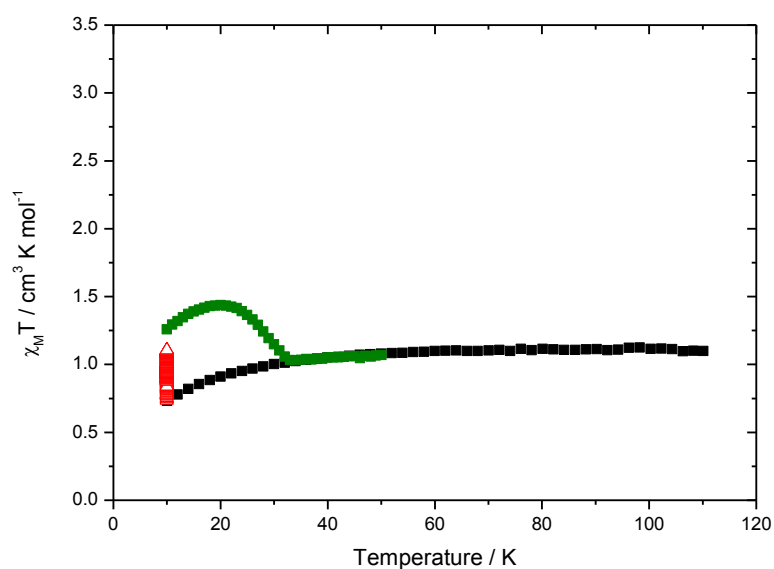


**Figure S9** Thermal behaviour of the  $\chi_M T$  product of **3** before irradiation ( $\blacksquare$ ), during irradiation ( $\blacktriangle$ ) and in the dark after irradiation ( $\blacksquare$ ). Note Photomagnetic measurement on a surface sample. Irradiation at 640 nm for 6 hours, three repeat measurements were made to try to improve the photoconversion efficiency without success. T(LIESST) = 30 K

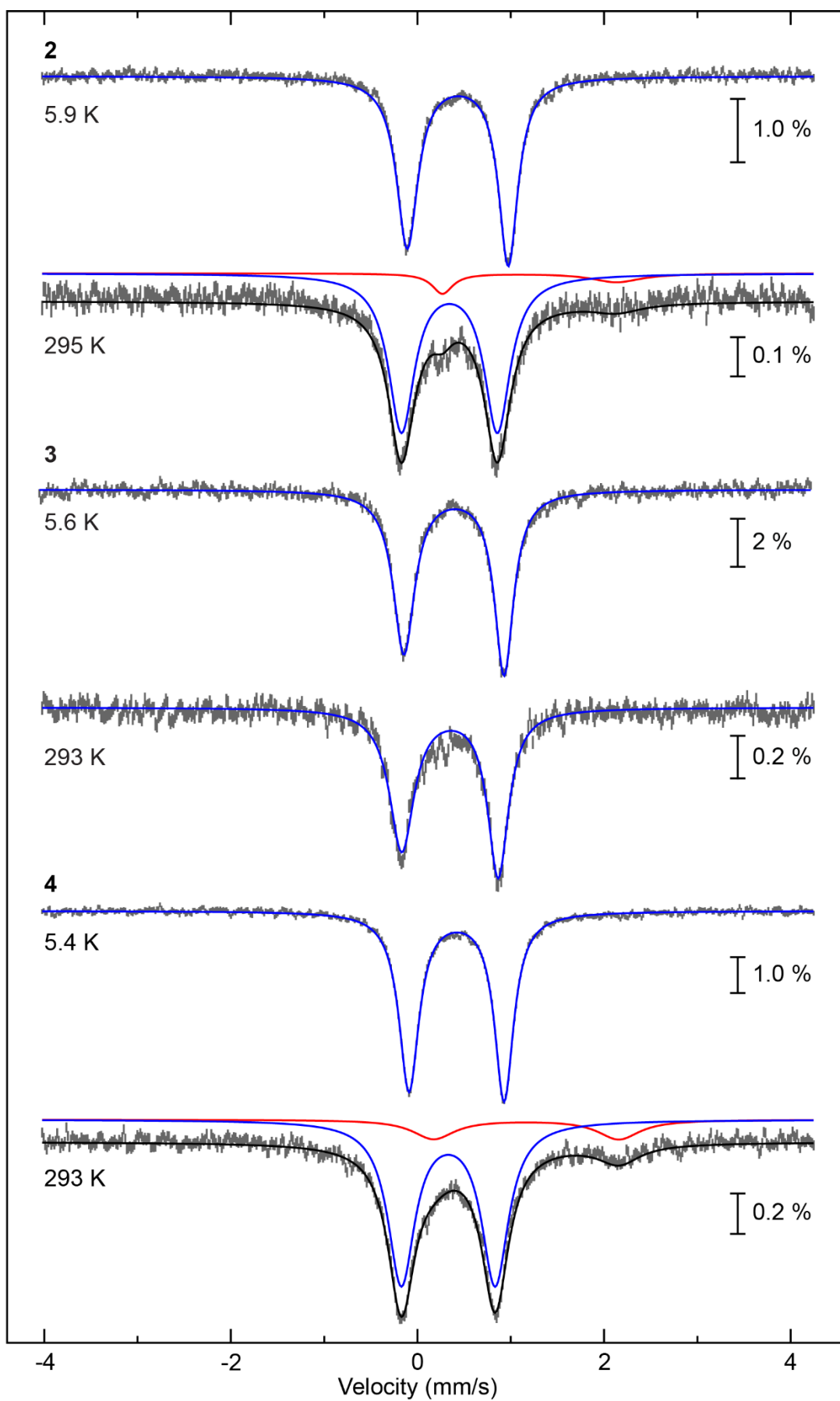


**Figure S10**  $^{57}\text{Fe}$  Mössbauer spectral plots for **2,3** and **4**. Velocity calibrations relative to  $\alpha$ -iron.

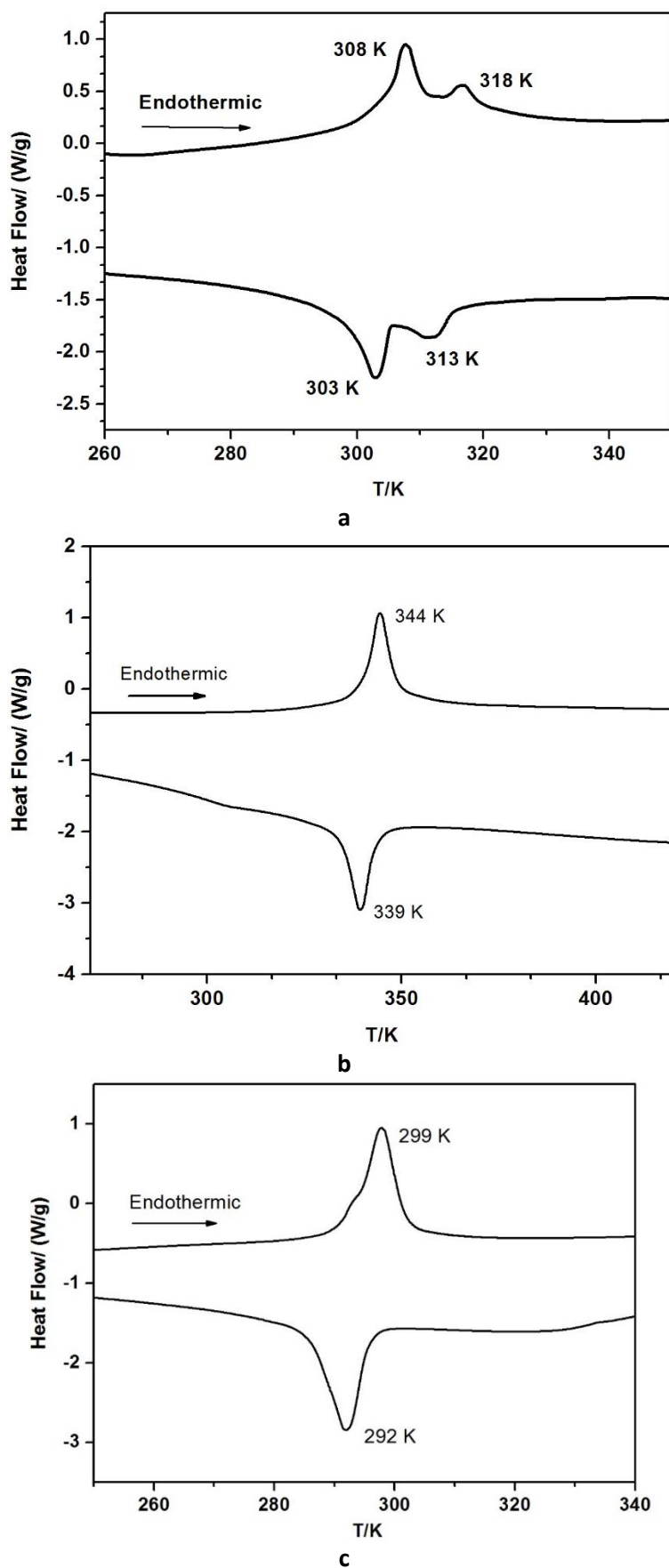


**Figure S11** DSC plots for compound a) **2**, b) **3** and c) **4**

**Table S9** Calculated  $\Delta H$  and  $\Delta S$  values from DSC results of the compounds **2**, **3**, **4**

Compound	$\Delta H/\text{J/mol}$		$\Delta S/\text{J/molK}$	
	Endo	Exo	Endo	Exo
<b>2</b>	5.7	6.0	18.5	19.8
<b>3</b>	16.5	15.0	48.0	44.2
<b>4</b>	8.2	8.2	27.4	28.0

**Table S10** B3LYP optimized selected bond parameters for complex **2-4** and **4'** (See Figure S1 for atoms labelling).

Bond Parameters	Complex 2					Complex 3				
	X-ray		HS	IS	LS	X-ray		HS	IS	LS
	100K	308K				100K	380K			
Fe-N1	1.939	2.001	2.180	1.970	1.971	1.942	2.137	2.188	1.974	1.978
Fe-N2	1.949	2.028	2.231	1.993	1.979	1.952	2.157	2.218	1.994	1.987
Fe-N3	1.956	1.995	2.180	1.970	1.970	1.946	2.133	2.188	1.973	1.978
Fe-N4	1.937	2.030	2.231	1.993	1.979	1.961	2.164	2.218	1.994	1.987
Fe-O1	1.955	1.968	2.055	1.892	1.966	1.944	2.007	2.033	1.894	1.971
Fe-O2	1.959	1.954	2.055	1.892	1.966	1.946	2.000	2.033	1.894	1.971
N2-Fe-O1	177.7		160.1	174.0	176.3	176.9		159.6	174.0	176.1
N4-Fe-O2	177.5		160.1	174.1	176.3	177.9		159.6	174.0	176.1

Bond Parameters	Complex 4					Complex 4'			
	X-ray		HS	IS	LS	X-ray	HS	IS	LS
	100K	298K							
Fe-N1	1.938	2.108	2.180	1.970	1.971	2.125	2.171	2.044	1.970
Fe-N2	1.949	2.126	2.215	1.992	1.979	2.152	2.192	2.255	2.006
Fe-N3	1.938	2.096	2.180	1.970	1.971	2.124	2.171	1.974	1.970
Fe-N4	1.949	2.132	2.215	1.992	1.979	2.145	2.192	2.038	2.006
Fe-O1	1.953	1.997	2.028	1.892	1.967	1.928	1.911	1.896	1.882
Fe-O2	1.957	2.017	2.028	1.892	1.967	1.930	1.911	1.964	1.882
N2-Fe-O1	177.5		159.9	174.3	176.3	165.2	159.6	165.2	174.6
N4-Fe-O2	177.4		159.9	174.3	176.3	164.6	159.6	170.5	174.5

The calculated low spin ( $S = 0$ ) structures of **2** - **4** and the high-spin ( $S = 5/2$ ) structure of **4'** are very similar to the X-ray structures. DFT calculations reveal that in complexes **2** - **4** and **4'**, the Fe-N distances in HS states are in the range of 2.17 to 2.23 Å while in the LS structures the bond lengths are in the range of 1.97 to 2.0 Å (Table 6). Similarly, the Fe-O distances in the HS states are in the range of 1.91 to 2.06 Å while in the LS structures the bond lengths are in the range of 1.88 to 1.96 Å.

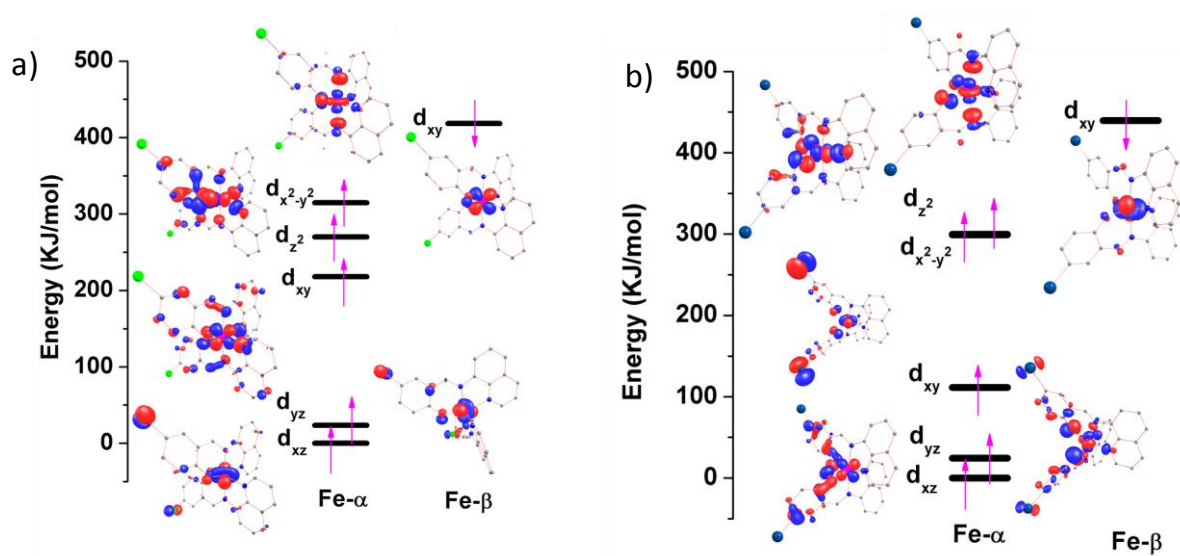


Figure S12 Eigenvalue plots computed for complexes a) **2** and b) **4**.

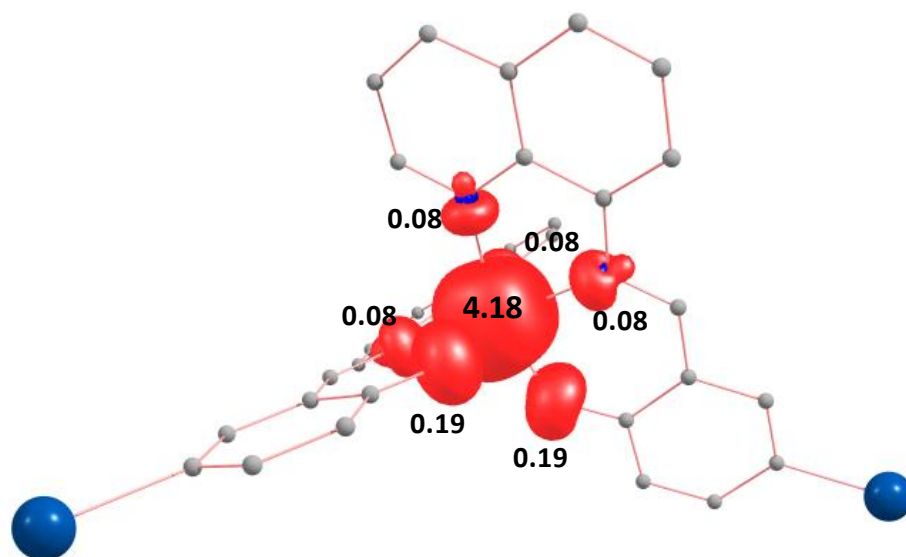


Figure S13 B3LYP computed spin density plot of the HS state for complex **4'**.

## Theory

The observed spin-crossover properties can be correlated by estimating  $\Delta S$  and  $T_{1/2}$  values, thus we have estimated these parameters for complexes **2** – **4**. The entropy change between the HS and LS spin states, *i.e.*  $\Delta S = S_{\text{HS}} - S_{\text{LS}}$  is found to be  $58.2 \text{ J mol}^{-1} \text{ K}^{-1}$ ,  $75.7 \text{ J mol}^{-1} \text{ K}^{-1}$ , and  $48.4 \text{ J mol}^{-1} \text{ K}^{-1}$  for **2**, **3**, and **4** respectively. These estimated energy gaps are comparable with the experimental reports for Fe spin crossover compounds.<sup>[10]</sup>

The  $T_{1/2}$  values are calculated from the electronic energy, vibrational and entropic contributions to the energy using the following equation as reported earlier.<sup>[11]</sup>

$$T_{1/2} = [\Delta E_{\text{el}}(0) + \Delta E_{\text{vib}}(T_{1/2})] / \Delta S(T_{1/2})$$

Here  $\Delta E_{\text{el}}(0)$  is the electronic energy difference between the high spin and low spin state along with the zero point energy correction and the thermal correction to electronic energy.  $\Delta E_{\text{vib}}$  is the vibration due to thermal energy of high spin and low spin state and  $\Delta S$  is the entropy of the system.

The vibrational and entropic contributions are computed from frequency calculations (See computational details). The  $\Delta E_{\text{el}}(0)$  energy in the above equation is considered to be the electronic energy with the zero point energy correction from calculations and this values (HS-LS) for complex **2**, **3**, and **4** are  $-3.5$ ,  $-5.7$  and  $-3.8 \text{ Kcal/mol}$  respectively. On the other hand the  $\Delta E_{\text{vib}}$  values are estimated to be  $-0.8$ ,  $-1.1$  and  $-0.07 \text{ Kcal/mole}$  for complex **2**, **3** and **4**. With these and the  $\Delta E_{\text{el}}$  energy, the  $T_{1/2}$  values are calculated to be  $310.1 \text{ K}$ ,  $373.2 \text{ K}$  and  $335.0 \text{ K}$  for complexes **2**, **3** and **4** respectively. The calculated results clearly reproduces the experimental  $T_{1/2}$  values, however the values are slightly overestimated for complexes **3** and **4** (See Table 4).

## References

- [1] D. J. Harding, W. Phonsri, P. Harding, K. S. Murray, B. Moubaraki, G. N. L. Jameson, *Dalton Trans.* **2015**, *44*, 15079-15082.
- [2] L. Zhang, G.-C. Xu, H.-B. Xu, T. Zhang, Z.-M. Wang, M. Yuan, S. Gao, *Chem. Commun.* **2010**, *46*, 2554-2556.
- [3] T. Kuroda-Sowa, Z. Yu, Y. Senzaki, K. Sugimoto, M. Maekawa, M. Munakata, S. Hayami, Y. Maeda, *Chem. Lett.* **2008**, *37*, 1216-1217.
- [4] T. Kuroda-Sowa, K. Kimura, J. Kawasaki, T. Okubo, M. Maekawa, *Polyhedron* **2011**, *30*, 3189-3192.
- [5] O. Iasco, E. Rivière, R. Guillot, M. Buron-Le Cointe, J.-F. Meunier, A. Bousseksou, M.-L. Boillot, *Inorg. Chem.* **2015**, *54*, 1791-1799.
- [6] C. M. Klug, A. M. McDaniel, S. R. Fiedler, K. A. Schulte, B. S. Newell, M. P. Shores, *Dalton Trans.* **2012**, *41*, 12577-12585.
- [7] L. Zhang, G.-C. Xu, H.-B. Xu, V. Mereacre, Z.-M. Wang, A. K. Powell, S. Gao, *Dalton Trans.* **2010**, *39*, 4856-4868.
- [8] L. Zhang, G.-C. Xu, Z.-M. Wang, S. Gao, *Eur. J. Inorg. Chem.* **2013**, *2013*, 1043-1048.
- [9] W. Phonsri, *Ph. D. Thesis, Walailak University, Thailand* **2014**.
- [10] J. M. Holland, J. A. McAllister, Z. Lu, C. A. Kilner, M. Thornton-Pett, M. A. Halcrow, *Chem. Commun.* **2001**, 577-578.
- [11] S. Ye, F. Neese, *Inorg. Chem.* **2010**, *49*, 772-774.